

Technical Report No. 32-380

*The Influence of Shape on Aerodynamic Damping
of Oscillatory Motion during Mars Atmosphere
Entry and Measurement of Pitch Damping at
Large Oscillation Amplitudes*

Bain Dayman, Jr.

James M. Brayshaw, Jr.

Duane A. Nelson

Peter Jaffe

Terry L. Babineaux

OTS PRICE

XEROX	\$	<u>3.60</u>
MICROFILM	\$	<u>1.37</u>



JET PROPULSION LABORATORY
CALIFORNIA INSTITUTE OF TECHNOLOGY
PASADENA, CALIFORNIA

February 28, 1963

Technical Report No. 32-380

*The Influence of Shape on Aerodynamic Damping
of Oscillatory Motion during Mars Atmosphere
Entry and Measurement of Pitch Damping at
Large Oscillation Amplitudes*

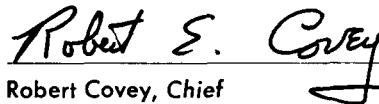
Bain Dayman, Jr.

James M. Brayshaw, Jr.

Duane A. Nelson

Peter Jaffe

Terry L. Babineaux



Robert Covey, Chief
Aerodynamic Facilities



Marcus G. Comuntzis, Acting Chief
Spacecraft Design

JET PROPULSION LABORATORY
CALIFORNIA INSTITUTE OF TECHNOLOGY
PASADENA, CALIFORNIA

February 28, 1963

**Copyright © 1963
Jet Propulsion Laboratory
California Institute of Technology**

**Prepared Under Contract No. NAS 7-100
National Aeronautics & Space Administration**

CONTENTS

I. Introduction	1
A. Mission Requirements	1
B. Major Influences on Entry Dynamics	2
C. Methods Used to Obtain Pitch Damping	2
II. Machine-Calculated Entry-Oscillatory-Motion Studies	4
A. Assumptions	4
B. Vehicle Parametric Constraints	4
C. Results of Trajectory Dynamic Studies	5
III. The Captive-Model Approach	10
A. The Gas Bearing	10
B. Model Support	10
IV. Captive-Model Data Reduction	16
A. Equation of Motion	16
B. Data Reduction	17
1. Complete, exact solution	17
2. Simplest solution	17
3. Compromise solution	18
V. Free Flight	19
VI. Typical Experimental Results	25
VII. Conclusions	29
Nomenclature	30
References	31

TABLES

1. Vehicle parametric constraints for the machine-calculated entry-oscillatory-motion studies	5
2. Comparison of effective average solution of oscillation amplitude decay with the exact solution	18
3. Location of center of gravity (experimental) for pitch-damping measurements	25
4. Corrected amplitudes	26
5. Amplitude decay rates	26

FIGURES

1. Sketch of model shapes	2
2. Effect of pitch damping on oscillation envelope (A-5 shape)	6
3. Effect of pitch damping on oscillation envelope (B-2 shape)	6
4. Effect of pitch damping on oscillation envelope (O shape)	6
5. Effect of pitch damping on oscillation envelope (P shape)	6
6. Effect of pitch damping on oscillation envelope (V-5 shape)	7
7. Effect of pitch damping on the envelope of oscillation at altitude 50,000 ft for various entry vehicle shapes	7
8. Sensitivity of oscillatory envelope variation caused by pitch damping of the various shapes	7
9. Estimated critical pitch damping as a function of the ratio $\left(\frac{C_{L\alpha}}{C_D}\right)_{\alpha=0}$	8
10. Effect of the ratio $\left(\frac{C_{L\alpha}}{C_D}\right)_{\alpha=0}$ on the envelope of oscillation between region of maximum deceleration and 50,000 ft altitude	8
11. Effects of vehicle shape on the pitch oscillation envelope (zero pitch damping)	9
12. A-2 model on cross-support gas bearing	11
13. A-5 model on sting-support gas bearing	12
14. Calibration sphere on sting-support gas bearing	12
15. Typical cross-support gas-bearing model damping data as recorded by the internal angle-of-attack readout system	13
16a. 16-mm motion pictures showing one-half cycle of oscillatory motion of A-5 model on sting-support gas bearing in hypersonic wind tunnel	14
16b. Typical sting-support gas-bearing model damping data as read from 16-mm motion picture film	15
17. Analytical example of local pitching moment and pitch damping	16
18. Analytical study of aerodynamic pitch damping	17
19. Definition of the amplitude rate of decay	17
20a. High speed motion pictures showing A-1 model during one-half cycle of flight in supersonic wind tunnel	20
20b. Angle of attack vs time, A-1 free-flight model (supersonic wind tunnel)	21
21a. High speed motion pictures showing A-1 model during one-half cycle of flight in hypersonic wind tunnel	22
21b. Angle of attack vs time, A-1 free-flight model (hypersonic wind tunnel)	23

FIGURES (Cont'd)

22. Enlargement of sample 35-mm half-frame pictures of A-1 model in flight	24
23. Average effective pitch damping vs oscillation amplitude	25
24. Six-degree-of-freedom data reduction for free flight trajectory of Fig. 20	25
25. Average effective pitch damping vs oscillation amplitude, cross-support gas bearing	26
26. Comparison of average effective pitch-damping gas bearing vs ball bearing	27
27. Sting-support gas-bearing damping as measured with a calibration sphere, at various Mach numbers	27
28. Comparison of gas-bearing damping (sting vs cross support) as measured with a calibration sphere	27
29. Sting-support gas bearing as measured with a calibration sphere, at various dynamic pressures	27

ACKNOWLEDGEMENTS

The efforts of the following, without which this study would not have been possible, are gratefully acknowledged: Donald C. Snyder for programming the six-degree-of-freedom equations-of-motion used in the atmosphere-entry investigations; Robert Hahn for designing and Henry J. Cools for building and checking out both gas-bearing supports used in the captive model pitch-damping tests; Alfred C. Conrad and George H. Walters for their patience and ingenuity in constructing the free-flight models; and Harold P. Holway and Warren J. Fife for engineering the equipment used to measure accurately the center-of-gravity locations and the moments-of-inertia of the small, light-weight free-flight models.

PREFACE

Various portions of this Report were presented at the American Astronautical Society Ninth Annual Meeting, held in Los Angeles, January, 1963, and at the Institute of Aerospace Sciences 31st Annual Meeting, held in New York City, January, 1963.

ABSTRACT

Preliminary mission requirements for first generation vehicles proposed for entry into the atmosphere of Mars indicate the use of a high-drag body of revolution with length about equal to the maximum diameter. Even for the case of initial rearward entry, it is desirable that forward orientation with low amplitudes of oscillation of such vehicles during the heating period (and beyond) be attained passively; that is, without the need of any active control devices. Six-degree-of-freedom atmosphere-entry studies indicate the significant effects of both vehicle shape and pitch damping upon the envelope of the angle-of-attack oscillation at the time of practical parachute deployment. One purpose of this Report is to demonstrate the importance of the vehicle shape upon the requirements (accuracy and angle-of-attack amplitude) for measuring pitch damping; the other purpose is to discuss the two wind tunnel methods being developed to measure small amounts of pitch damping accurately at high amplitudes of oscillation.

I. INTRODUCTION

A. Mission Requirements

Certain tentative mission, aerodynamic, weight, reliability, and packaging requirements for vehicles proposed for entry into the atmosphere of Mars suggest the use of a high-drag body of revolution with length approximately equal to the maximum diameter. Since such capsules may be passive in their method of stabilization, they must be unstable in a rearward direction and will

oscillate during penetration into the planetary atmosphere.

For the purposes of mission planning, the vehicle's least desirable initial entry attitudes (vehicle's angle of attack at some reference altitude, and the spin and pitch rates) must be determined, for they become a basis for the design criteria. Six-degree-of-freedom atmosphere-

entry motion studies (Ref. 1) indicate that an initial rearward orientation (with no spin or initial pitch rate) of the A-2 vehicle shown in Fig. 1 gives the largest oscillation-amplitude envelope during the entire entry.

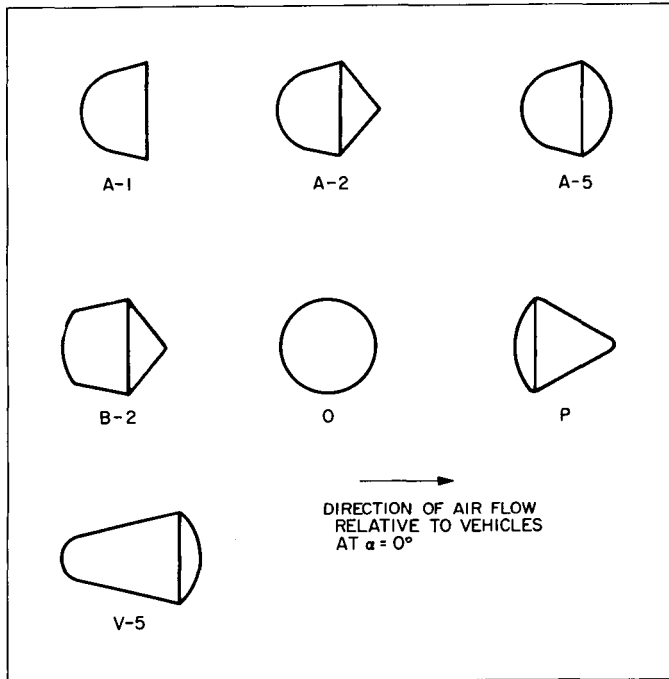


Fig. 1. Sketch of model shapes

Because the vehicle is likely to be initially misaligned relative to its flight path, it will oscillate in angle of attack along its entry trajectory. This angular motion, which is superimposed upon the mean flight path, is of concern for the following reasons: it affects the loads and load distribution on the vehicle; it determines the portions of the vehicle surface which will be exposed to the most severe heating conditions; it determines the ability of the vehicle to perform in-flight operations, such as data transmission, atmosphere sensing, aimed observations, and, if used, parachute deployment.

B. Major Influences on Entry Dynamics

Reference 2, although based upon simplified linearizations of the actual complex equations of motion, adequately illustrates the relative importance of the various factors which affect the oscillatory motion of a vehicle during atmosphere entry. The linearization does not mask the relative importance of the various items, and, if a proper weighting factor is used (Ref. 3), a fairly reliable magnitude of the oscillatory motion during the terminal phase of the entry trajectory can be calculated.

For the purposes of this Report, only two of the many items affecting entry dynamics were investigated, namely, vehicle shape and pitch damping. The effects of variation of the following were not investigated: planetary atmosphere and gravity; initial velocity or flight-path-angle relative to the planet; magnitude of initial misalignment between vehicle and flight path; vehicle size, weight, center of gravity, and moment of inertia. In fact, the vehicle shapes were limited to a few specific nonlifting bodies of revolution with no regard for obtaining an orderly, mathematical variation in the vehicle's static aerodynamic characteristics.

The static aerodynamic characteristics, which are determined by a vehicle's shape, are generally quite easy to obtain; except for the V-5 shape discussed later in this Report, they were measured experimentally. As these experimental measurements compared very favorably with modified Newtonian calculations, the Newtonian approach was used for the V-5 shape. However, dynamic aerodynamic characteristics are not usually a simple matter to obtain, and precise experimental means are required to determine dynamic data such as pitch damping.

In order to have a guide in planning experimental measurements of pitch damping, several types of information are required: the approximate magnitude of the pitch damping [this can be estimated from Newtonian flow calculations in conjunction with previous experimental results; anomalies in both magnitude and sign are prevalent (See Ref. 4)]; the amplitude of oscillation during which pitch damping can affect the oscillatory motion; and the sensitivity of the oscillatory motion to pitch damping. Except for one specific shape, this Report does not go into the expected pitch damping of a shape, but does consider the latter of two types of information required.

Differences in the oscillatory behavior during entry into one specific assumed atmosphere of Mars and for a number of entry-vehicle shapes will be investigated by means of machine-calculated motion histories, and discussions of the findings will be made.

C. Methods Used to Obtain Pitch Damping

In the past, the primary methods for obtaining pitch damping utilized the sting-flexure mounted, wind-tunnel models and the ballistic range models. Although the data repeatability is good for the forced-oscillation (sting-flexure) models, the angles of attack are generally limited

to below 20 deg.¹ Not only are the range data usually limited to small angles of attack, but the data repeatability is considerably poorer than for sting-flexure mounted models. However, range data do not have any support interference effects, which can be a very important consideration. Many experiments have shown that the model base shape can have an effect upon the pitch damping (Ref. 5, 6). This would indicate that the presence of a sting may also have an effect. Perhaps the base and sting effects upon the pitch damping are important only at the lower Mach numbers ($M < 3$), but this must be demonstrated for each model shape investigated.

Ball bearings have been used for both cross-supported and sting-supported models (Ref. 7, 8), but unfortunately they have damping friction comparable to the expected aerodynamic pitch damping for short, blunt vehicle shapes. Preliminary experimental work at the Jet Propulsion Laboratory indicated that ball bearings were adequate for $M = 2$ with $\alpha_{\max} > 30$ deg, marginally satisfactory for $M = 3$ with $\alpha_{\max} > 60$ deg, and totally inadequate for $M > 4$. Even though the ball-bearing friction is small enough to make it possible to obtain some

meaningful aerodynamic pitch-damping data at the lower Mach numbers ($M < 2$), the effects of support interference upon the data are probably appreciable.

In order to fulfill the high angle of oscillation and anticipated small pitch-damping measurement requirements, it was decided to use two different approaches: (1) To mount the models on a gas bearing which was supported by a cross-support, permitting angles of oscillation from 0 to 180 deg, and on a sting mount which restricted the maximum angle of attack to about ± 45 deg for the blunter shapes shown in Fig. 1; and (2) To free-flight models in a wind tunnel. The damping friction of the gas bearing was expected to be within the tolerance to which the aerodynamic pitch damping of the models should be determined. The free-flight method would yield typical single-plane motion data which could be reduced to give sufficiently accurate pitch damping, but the observed motion would be the true motion; that is, there would be no support interference. The free-flight technique requires laborious data reduction which probably would not have the repeatability and convenience of the captive gas-bearing data, but which would serve as a basis for determining the degree of support interference for the gas-bearing configurations. Also, the free-flight techniques could give visual indication of the vehicle motion to be expected during the final phases of atmospheric entry.

¹The use of an off-set center of gravity or a trim surface makes it practical to obtain data at higher angles of attack, but the effects of such approaches upon the desired data must be determined.

II. MACHINE-CALCULATED ENTRY-OSCILLATORY-MOTION STUDIES

A. Assumptions

Static aerodynamic coefficients invariant with actual Mach number are used throughout the trajectory. Comparisons between calculated trajectories using both fixed and Mach-variant static coefficients for the A-2 shape showed differences in envelope amplitude of less than 5 deg down to $M = 2$. This point in the trajectory is well past maximum heating and loads and is in the region where retardation-system deployment is practical.

In order to show the effects of stabilizing or destabilizing amounts of pitch damping, $(C_{m_q} + C_{m_{\dot{\alpha}}})$ is held constant throughout each trajectory.² This procedure is repeated for several arbitrary values of $(C_{m_q} + C_{m_{\dot{\alpha}}})$. Thus the degree of importance of pitch damping on resultant motion may be assessed without needing actual $(C_{m_q} + C_{m_{\dot{\alpha}}})$ values as functions of α , M , and R_D , which are presently unknown for most of these shapes and whose values might vary by small but critical amounts in an actual flight because of conditions not specified in the machine calculation.

The equations of motion are the six-degree-of-freedom equations assuming a rigid body and an atmosphere fixed to the planet. They are written in detail in Ref. 1. The assumed Mars atmosphere is

$$\rho = \rho_0 \exp(-\beta y)$$

where

$$\rho_0 = 0.409 \times 10^{-3} \text{ slug/ft}^3$$

$$\beta = 2.42 \times 10^{-5}/\text{ft}$$

The vehicle initial entry conditions are taken to be

$$V_E = \text{entry velocity} = 25,000 \text{ ft sec}^{-1}$$

$$\theta_E = \text{entry angle} = 90 \text{ deg. (i.e., vertical to planet surface)}$$

$$\text{pitch, yaw, and roll rates} = 0$$

$$\alpha_E = \text{Angle of attack} = 179 \text{ deg}$$

This near-maximum condition is expected to produce maximum amplitude sensitivity to differences in shape characteristics. The aerodynamic stability coefficients determined in air are assumed to be applicable for the atmosphere of Mars.

² $(C_{m_q} + C_{m_{\dot{\alpha}}})$ is treated as equivalent to C_{m_q} in the equations of motion.

B. Vehicle Parametric Constraints

The choice of the five vehicle shapes was quite arbitrary. The A-5, B-2, and O shapes are being considered because of the compactness of shape and the high drag coefficient—both highly desirable properties. The A-5 forebody is a short, blunted cone. The B-2 shape is somewhat blunter in order to obtain a higher drag coefficient for a possible Mars atmosphere entry mission. The O shape is simply a sphere with a center of gravity off-set from the center. This zero-lift slope shape would follow a straight trajectory and would possibly make the interpretation of data from internal accelerometers less formidable than for other vehicle shapes. The P shape, similar to several proposed Earth re-entry vehicles, was picked in order to have a lower limit on the lift-curve slope. Likewise, the V-5 shape was investigated in order to have an upper limit on the lift-curve slope.

In order to isolate the effects of shape on the oscillatory motion, some method of holding static-stability shape effects to a minimum appeared desirable. Reference 2 derives a closed-form approximate solution for small angle-of-attack oscillations of an entry vehicle. Now, in all the cases investigated herein, an initial α_E of 179 deg is chosen to afford the largest sensitivity to envelope changes between shapes. Convergence in an α_{env} from the maximum α_E implies convergence to a lower α_{env} for any lesser α_E . This is shown theoretically in Ref. 2 and verified by the machine calculations of Ref. 1. Although α_{env} is initially high in this study, it rapidly decreases to much lower values, especially in the high deceleration region where the effect of pitch damping begins to change the oscillatory envelope. Thus the theory of Ref. 2 is used as a guide in determining the vehicle parameter constraints necessary to hold static-stability parameters nearly the same for all of the shapes while allowing dynamic stability to change with shape.

Reference 2 gives simple expressions for the envelope amplitude, (α_{env}/α_E) , and oscillation frequency f , wherein the only aerodynamic shape-governed factors are K_1 and K_2 in α_{env}/α_E and K_0 and K_2 in f .

$$\frac{\alpha_{env}}{\alpha_E} = \frac{\exp(K_1 e^{-\beta y})}{\left[\pi (K_2)^{\frac{1}{2}} \exp\left(-\frac{\beta y}{2}\right) \right]^{\frac{1}{2}}} \quad (1)$$

Table 1. Vehicle parametric constraints for the machine-calculated entry-oscillatory-motion studies

Common to all					
Moment of inertia about pitch axis = 5.6 slug ft ²					
All shapes are bodies of revolution with center of gravity on axis of symmetry					
Maximum diameter = 3.25 ft					
Ballistic coefficient $m/C_D A = 1.16$ slugs/ft ² at $\alpha = 0$					
Static pitching moment $C_{m\alpha} = -0.104/\text{rad}$ at $\alpha = 0$					
Individual					
Shape	Mass, slugs	cg location, d from nose	$C_{L\alpha}$ $\alpha = 0$	C_D $\alpha = 0$	$C_{L\alpha}/C_D$ $\alpha = 0$
A-5	6.68	0.42	+0.29	0.72	+0.41
B-2	8.59	0.37	-0.10	0.90	-0.11
O	8.88	0.39	0	0.93	0
P	14.33	0.20	-1.3	1.45	-0.89
V-5	3.15	0.67	+1.2	0.34	+3.44

$$f = \frac{\beta V_E (K_2)^{\frac{1}{2}} \sin \theta_E}{2\pi} \exp\left(-\frac{K_0}{2} e^{-\beta y}\right) \exp\left(-\frac{\beta y}{2}\right) \quad (2)$$

where

$$K_0 = \frac{\rho_0}{\beta \sin \theta_E} \frac{C_D A}{m} \quad (3)$$

$$K_1 = \frac{\rho_0}{4\beta \sin \theta_E} \frac{C_D A}{m} \times \left[1 - \frac{C_{L\alpha}}{C_D} + \frac{(C_{m_q} + C_{m_{\dot{\alpha}}})}{C_D} \frac{m}{I} d^2 \right] \quad (4)$$

$$K_2 = -\frac{\rho_0}{2\beta^2 \sin^2 \theta_E} \frac{Ad}{I} C_{m\alpha} \quad (5)$$

From these formulae it may be seen that K_1 controls the envelope convergence with altitude, and may accordingly be called a dynamic stability factor. On the other hand, K_2 may be called a static stability factor.

In order to isolate dynamic damping effects on each trajectory, variations in static stability are minimized by choosing vehicle parameters such that K_0 and K_2 do not vary from shape to shape.

For all shapes, I and d , respectively, are identical. By manipulation of the center of gravity, $C_{m\alpha}$ is the same for all shapes. Thus, static stability is invariant with shape for small α . Approximate entry translation theory (Ref. 9)

indicates that velocity vs altitude history is a function only of $m/C_D A$ for $\alpha_{env} = 0$. In this study, $m/C_D A$ and, consequently, K_0 is held identical for all shapes by varying the mass from shape to shape. Thus, the dynamic pressure history (main source of oscillatory energy) will remain about the same for all shapes examined, except for projected area differences due to angle of attack. Accordingly, differences in oscillation history between shapes will emphasize effects due to differences in K_1 . Looking within K_1 , the effect of the term $C_{L\alpha}/C_D$ will be isolated for those cases where $(C_{m_q} + C_{m_{\dot{\alpha}}})$ is set equal to zero. The vehicle parameter constraints are listed in Table 1 along with values of the static aerodynamic coefficients at $\alpha = 0$.

C. Results of Trajectory Dynamic Studies

A complete description of the results of this study, such as heating, acceleration, dynamic pressure, etc., would be beyond the purpose of this Report. Accordingly, results are restricted to presentation of the body-orientation aspects of the trajectories, as influenced by the various shapes.

Figures 2 through 6 show, for each of the shapes, the effect of arbitrary amounts of constant $(C_{m_q} + C_{m_{\dot{\alpha}}})$ upon the angle-of-attack oscillation envelope. Each curve corresponds to a complete trajectory, starting with near-backward entry at an altitude of 800,000 ft in the Mars atmosphere, and continuing down to around 40,000 ft. No envelope is plotted below a Mach number of 3. In

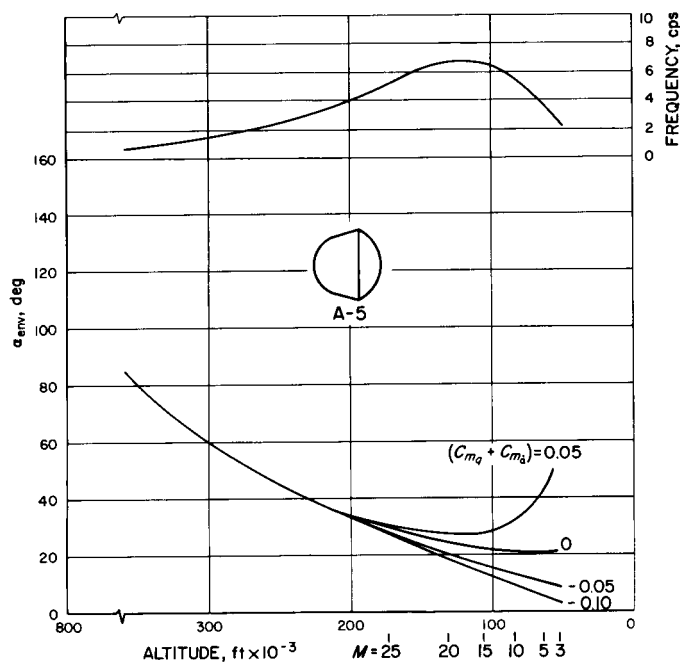


Fig. 2. Effect of pitch damping on oscillation envelope (A-5 shape)

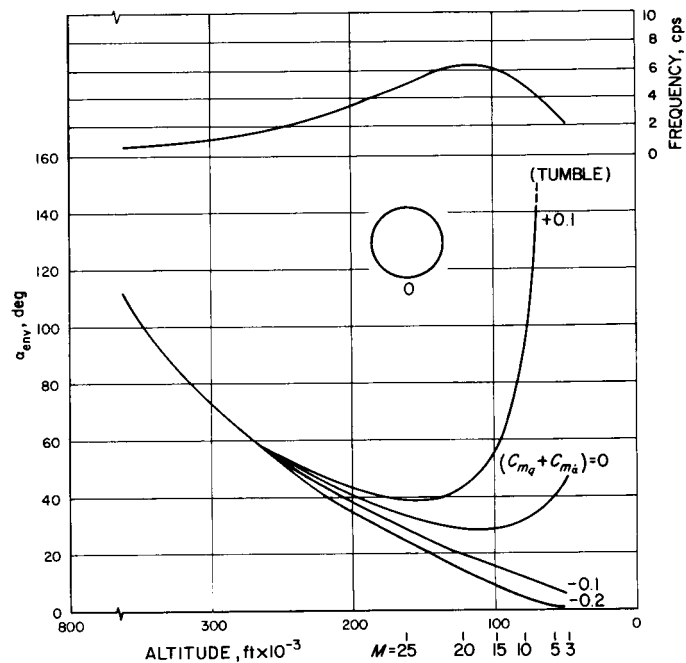


Fig. 4. Effect of pitch damping on oscillation envelope (O shape)

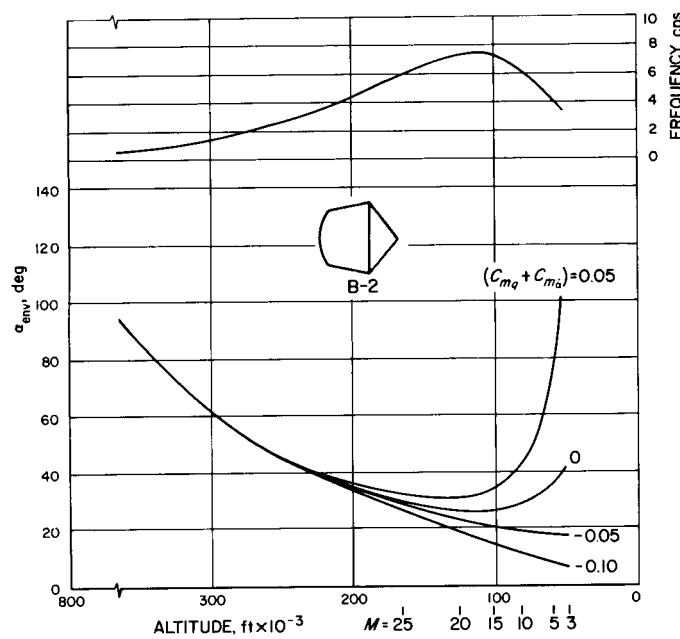


Fig. 3. Effect of pitch damping on oscillation envelope (B-2 shape)

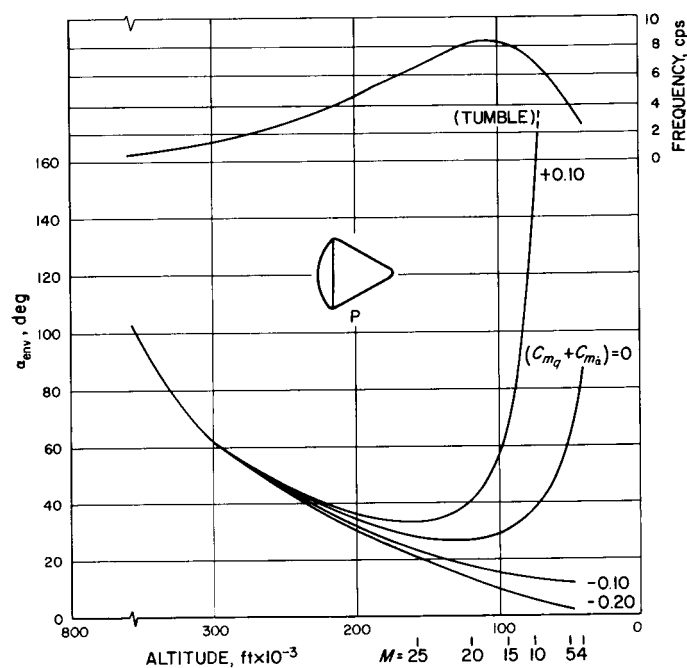


Fig. 5. Effect of pitch damping on oscillation envelope (P shape)

some of the cases using destabilizing $(C_{m_q} + C_{m_{\dot{\alpha}}})$ in the equations of motion, tumbling ($\alpha_{env} > 180$ deg) occurred before $M = 3$, and the curve was terminated at that point. The corresponding oscillation frequency is

also shown in these figures for the case of zero pitch damping. The frequency was not appreciably different for the other cases.

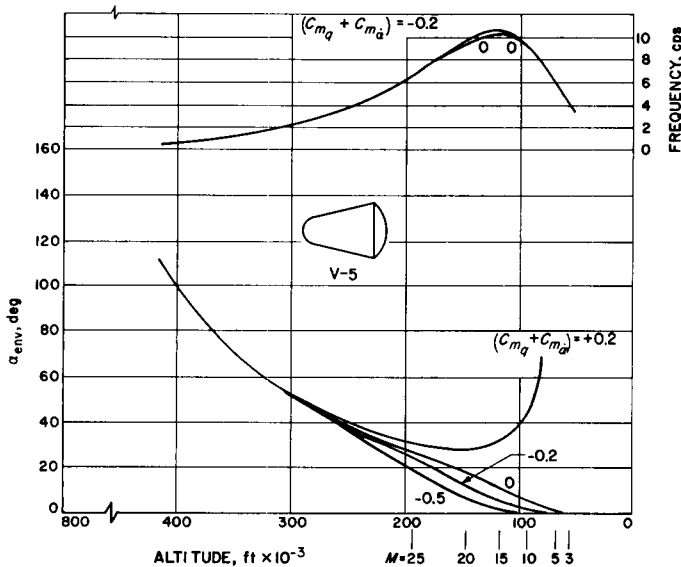


Fig. 6. Effect of pitch damping on oscillation envelope (V-5 shape)

The effect of pitch damping on the oscillatory envelope at an altitude of 50,000 ft for each of the shapes investigated is shown in Fig. 7. Of major importance in connection with the pitch damping measurement techniques described in Sections III and V is the indication in this Figure of the amplitude and accuracy required in the experimental measurements of $(C_{m_q} + C_{m_{\dot{\alpha}}})$ for each

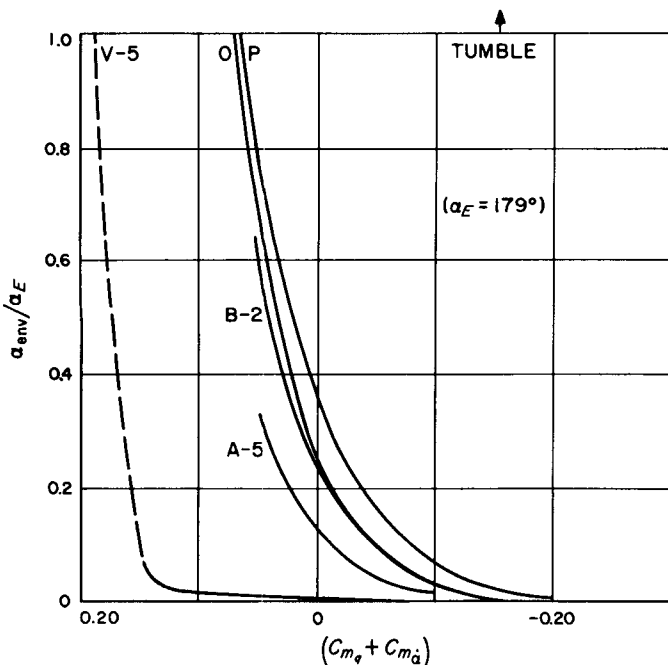


Fig. 7. Effect of pitch damping on the envelope of oscillation at altitude 50,000 ft for various entry vehicle shapes

shape. The sensitivity of a change in the oscillatory envelope of the various shapes at an altitude of 50,000 ft for a 0.01 change in $(C_{m_q} + C_{m_{\dot{\alpha}}})$ is shown in Fig. 8 in the case of $(C_{m_q} + C_{m_{\dot{\alpha}}}) = 0$. It is evident that some shapes are more sensitive to a given change in pitch damping than are others. As can be seen from Fig. 2 to 6, some shapes require more pitch damping in order to avoid angle-of-attack divergence after maximum deceleration than do others.

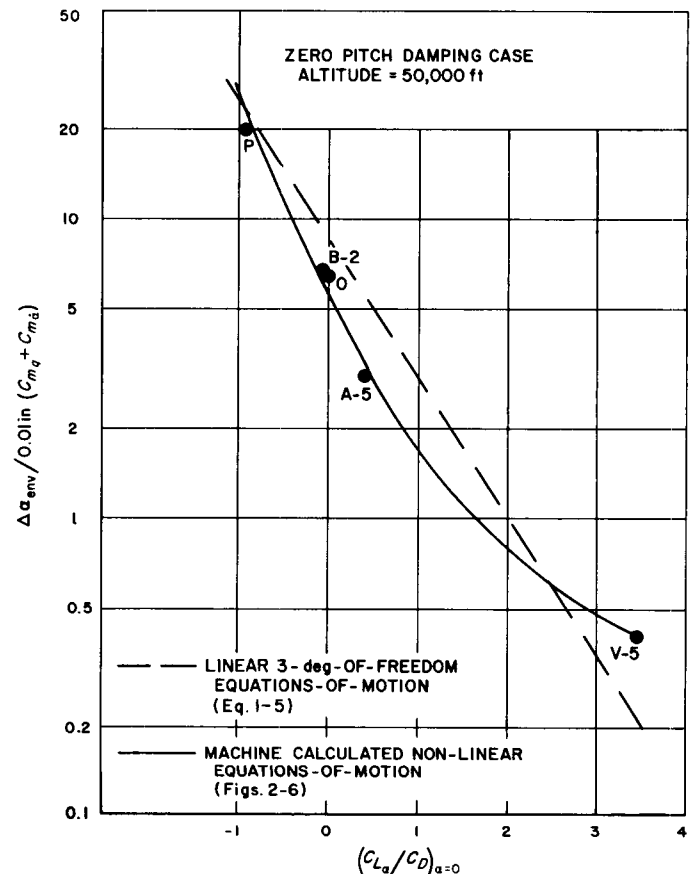


Fig. 8. Sensitivity of oscillatory envelope variation caused by pitch damping of the various shapes

The machine-calculated nonlinear equations-of-motion data in Fig. 8 are compared with similar data obtained from the linearized three-degree-of-freedom equations-of-motion (Eqs. 1-5). The linearized solution uses the $\alpha = 0$ deg dimensionless coefficients of Table 1, and the resulting amplitudes at 50,000 ft altitude are multiplied by the factor of two suggested in Reference 3. As can be seen, the simple linearized equations-of-motion give a reasonable result for determining the accuracy required for experimental measurements of pitch damping.

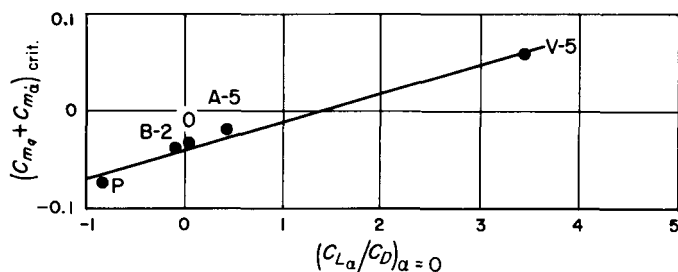


Fig. 9. Estimated critical pitch damping as a function of the ratio $\left(\frac{C_{L\alpha}}{C_D}\right)_{\alpha=0}$.

Figure 9 shows the critical damping $(C_{m_q} + C_{m_{\dot{\alpha}}})_{crit}$ requirements of each shape versus the ratio $C_{L\alpha}/C_D$. Critical damping is arbitrarily defined as the amount of pitch damping (positive or negative) which would have to exist in order to yield zero slope of α_{env} at an altitude of 50,000 ft ($M \approx 3$). As would be expected, shapes with the least $C_{L\alpha}/C_D$ require increasing amounts of stabilizing (negative) pitch damping to avoid α_{env} divergence. This curve represents a divergence boundary in the sense that, within configuration constraints imposed, any shape

must have an effective $(C_{m_q} + C_{m_{\dot{\alpha}}})$, which, when plotted vs $C_{L\alpha}/C_D$, falls on or below the curve if divergence is to be avoided prior to an altitude of 50,000 ft.

As described in Sections III and V, a continuing experimental program to determine actual pitch damping of these shapes is in progress. The actual $(C_{m_q} + C_{m_{\dot{\alpha}}})$ value may be found sufficient to forestall low speed α_{env} divergence. If not, the difference between a shape's intrinsic $(C_{m_q} + C_{m_{\dot{\alpha}}})$ and $(C_{m_q} + C_{m_{\dot{\alpha}}})_{crit}$ could be supplied by an active damping system, if that shape, for other reasons, were chosen for an entry vehicle.

Figure 10 indicates the fractional α_{env} divergence from maximum deceleration to 50,000 ft altitude, vs $C_{L\alpha}/C_D$ for each shape, assuming zero damping. Again those shapes with low plunge damping ($C_{L\alpha}/C_D \leq 0$) exhibit the most divergence. Figure 11 is a composite of the oscillatory envelopes of the vehicles in Fig. 2 to 6 for the assumed case of zero pitch damping showing differences in terminal divergence due mainly to the plunging stability term, $C_{L\alpha}/C_D$, for each shape.

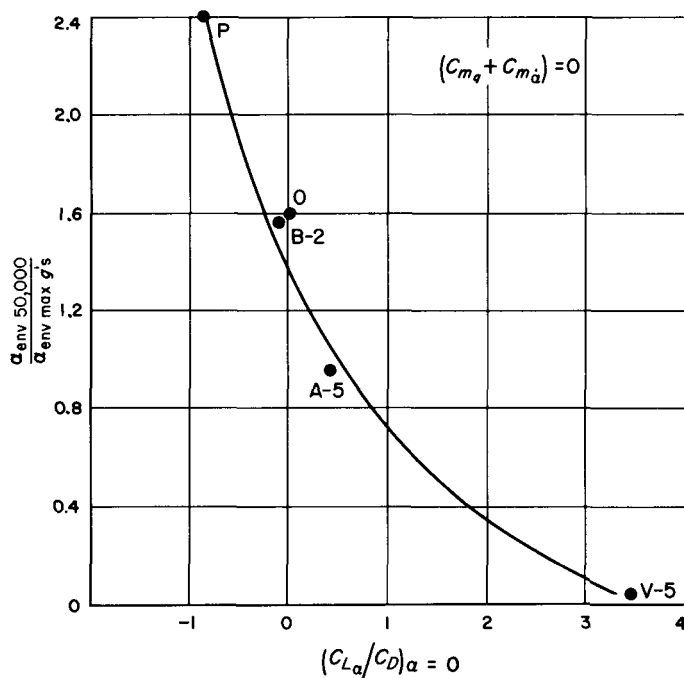


Fig. 10. Effect of the ratio $\left(\frac{C_{L\alpha}}{C_D}\right)_{\alpha=0}$ on the envelope of oscillation between region of maximum deceleration and 50,000 ft altitude

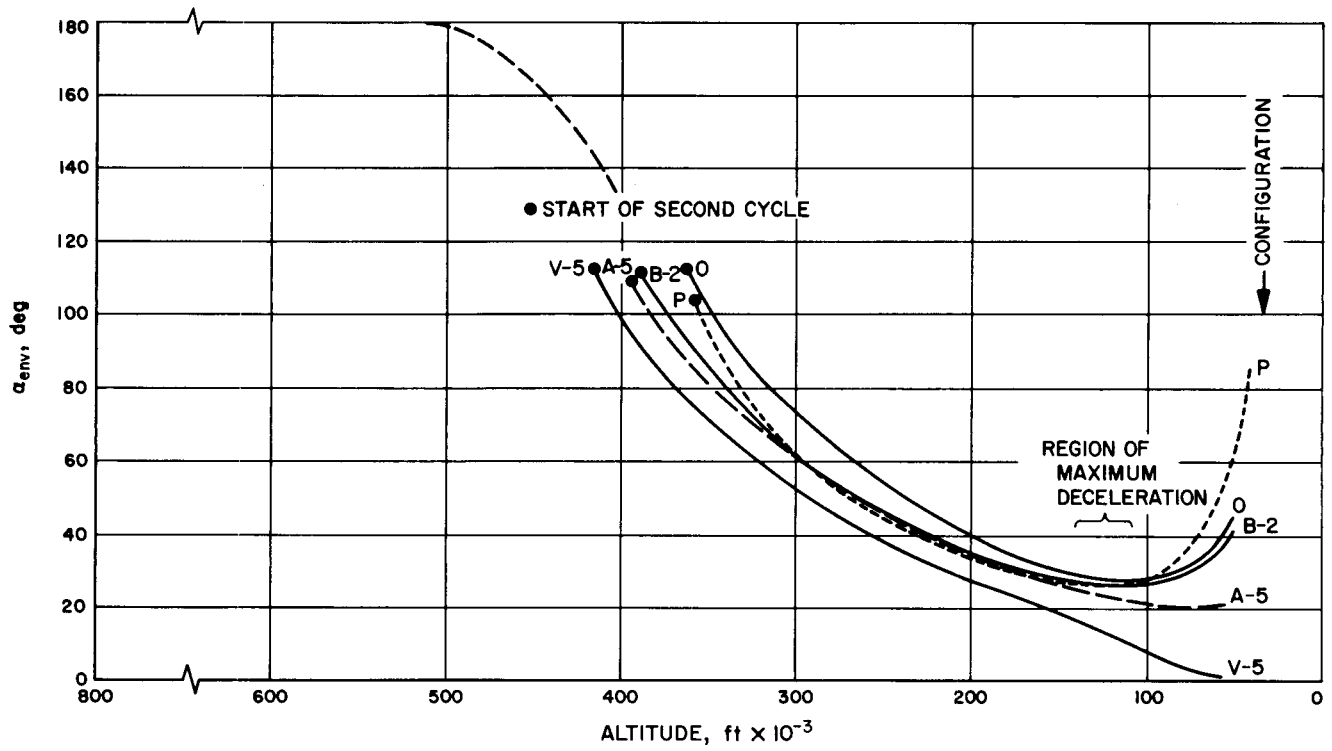


Fig. 11. Effects of vehicle shape on the pitch oscillation envelope (zero pitch damping)

III. THE CAPTIVE-MODEL APPROACH

A. The Gas Bearing

The gas bearings used in the determination of dynamic damping of these blunt bodies are quite similar to the ones used for gyroscope mounting. The cross-support configuration requires that the bearing housing rotates while the shaft remains fixed—the opposite to a normal gas bearing. But the sting-supported gas bearing is conventional in that the shaft rotates while the housing remains fixed. Reference 10 describes the gas bearing itself with details of the automatic angle-vs-time readout system which is mounted within the model. Experience has shown that it is unsatisfactory to have the bearing mounted laterally unsymmetrical with respect to the model because high model angular velocities put a twisting moment on the bearing which would prematurely ground out the bearing at the higher angles of oscillation ($\alpha_{\max} > 90$ deg).

The original gas bearing (for the cross support shown in Fig. 12) can support 20 lb of force in a direction radial to the bearing, while the newer bearing (for the sting support shown in Fig. 13) can support about 50 lb. Both bearings are 1 in. in diameter, 2 in. long, and have approximately a 0.0005-in. radial gap. The frictional damping of the gas bearings was experimentally measured under actual test conditions by mounting a thin shell sphere symmetrically on the bearing (Fig. 14). With tunnel flow established over this calibration sphere, the oscillation history of the sphere was recorded, this oscillation being caused by an off-center weight inside the sphere.³ The pitch damping measured in this way is quite repeatable and small compared with the damping of the models tested, as will be shown later.

In order to permit the testing of smaller models on the gas bearing, the internal, automatic, angle-of-attack read-

out was removed, making it necessary to rely on 16-mm motion pictures for recording the history of the oscillatory motion. Figure 15 is an example of the motion up to very high amplitudes for a model on the cross-supported gas bearing, as recorded by the internal angle-of-attack readout system. Figure 16 shows an example of one-half cycle of motion of a model on the sting-supported gas bearing, the data being recorded on 16-mm motion picture film. These optical data were used to obtain the $\Delta\alpha/\alpha_{\max}$ and frequency vs α_{\max} curves in this Figure. For both of these cases, the average effective pitch damping at each α_{\max} was derived from the smoothed graphical data by use of Eq. (15).

B. Model Support

As was previously mentioned, two types of supports for the gas bearings have been tried; the cross support and the sting support. Although the cross support does appear to have the possibility of large interference on the flow about the model, some wind-tunnel data (Ref. 11 and 7) indicate negligible interference for Mach numbers in excess of $M = 3$. For the most part, the region of interference from the cross support is restricted to the sides of the aft portion of the model, where the aerodynamic forces in the pitch plane are probably minor for the class of models in this Report. For obtaining damping data at high angles of oscillation, such a support is required. However, the assumption of negligible effect of the cross support on the pitch damping must be investigated for each basic model shape tested. Work performed (Ref. 12) on the interference of a single wire support (up to 2½% of model diameter) for both spheres and cones clearly demonstrated large changes of the wake shape relative to a no-support condition (model in free flight). A sting support would be required for certain shapes of models where the cross support would interfere with flow over the face of the model. Also, for Mach numbers from $M = 3$ through the transonic region, a sting support would be preferable to a cross support. However, as the base shape of the model has an important effect upon the damping moment for $M < 3$, it is probable that the presence of the sting itself would affect the damping data.

³The reason for using a light-weight, low-moment-of-inertia calibration sphere was to take advantage of the tunnel air flow for putting loads on the gas bearing of the same magnitude that would occur with a model, at the same time maintaining a frequency of oscillation similar to that for a model. The use of the usual nonaerodynamic, dead-load means for loading the gas bearing to 50 lb would result in a (comparatively) very low frequency of oscillation due to the very high moment of inertia of such a load.

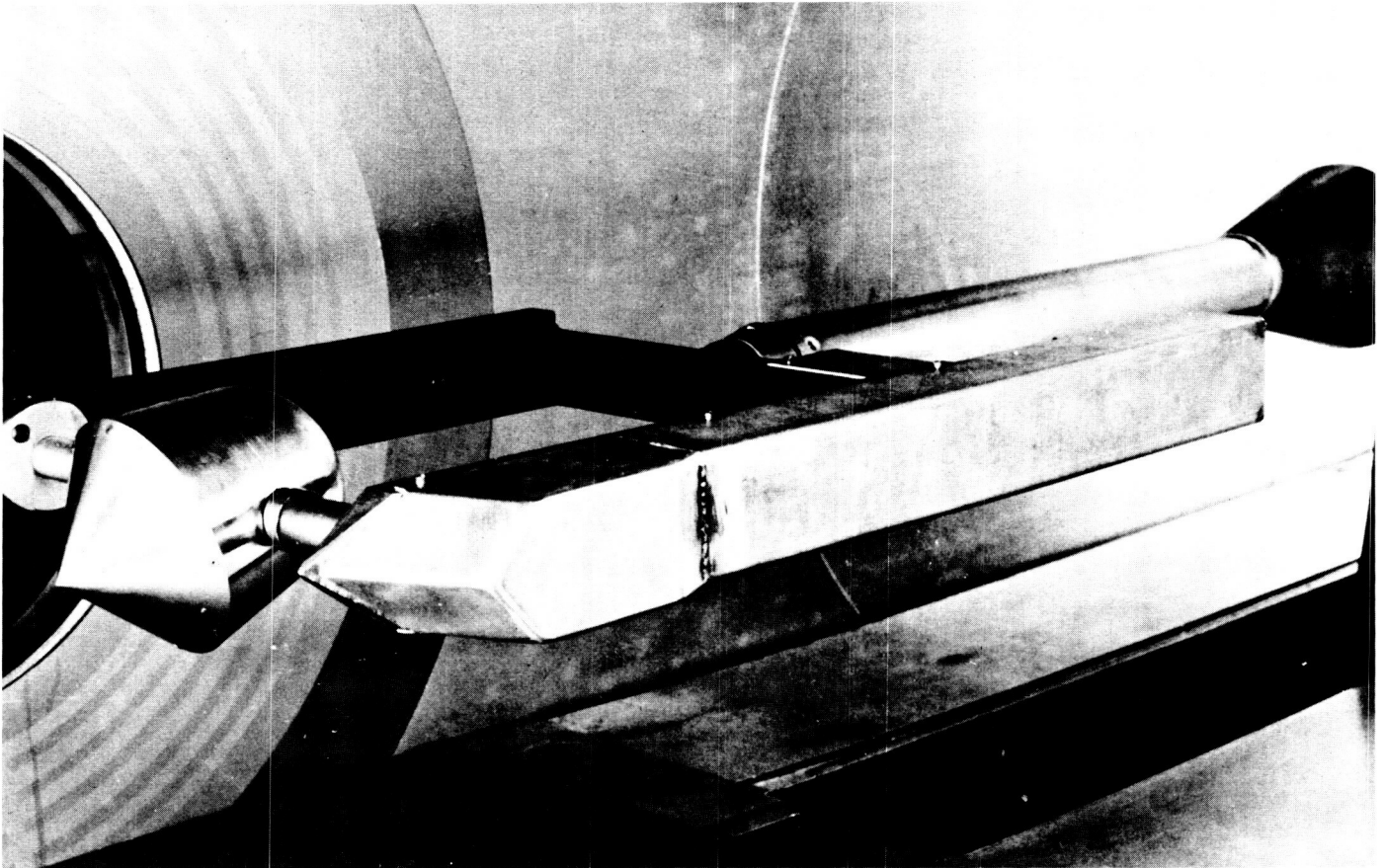


Fig. 12. A-2 model on cross-support gas bearing

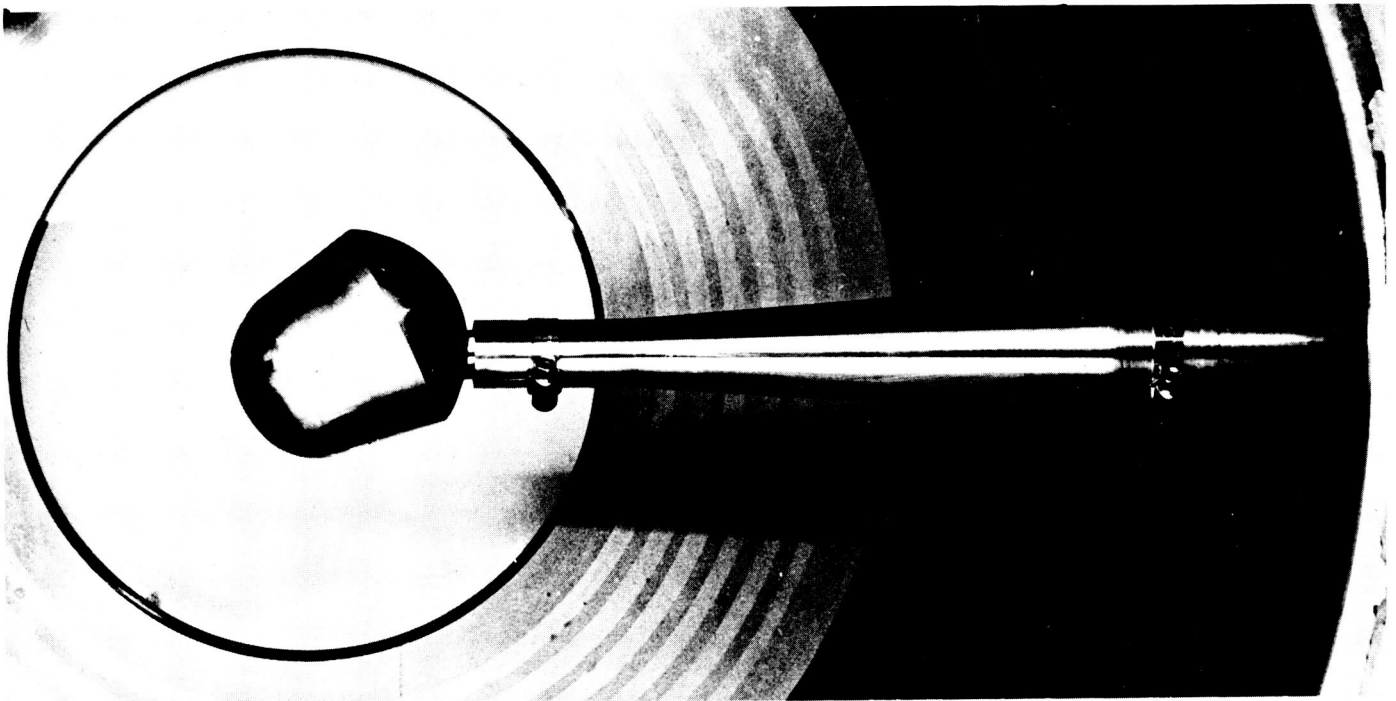


Fig. 13. A-5 model on sting-support gas bearing

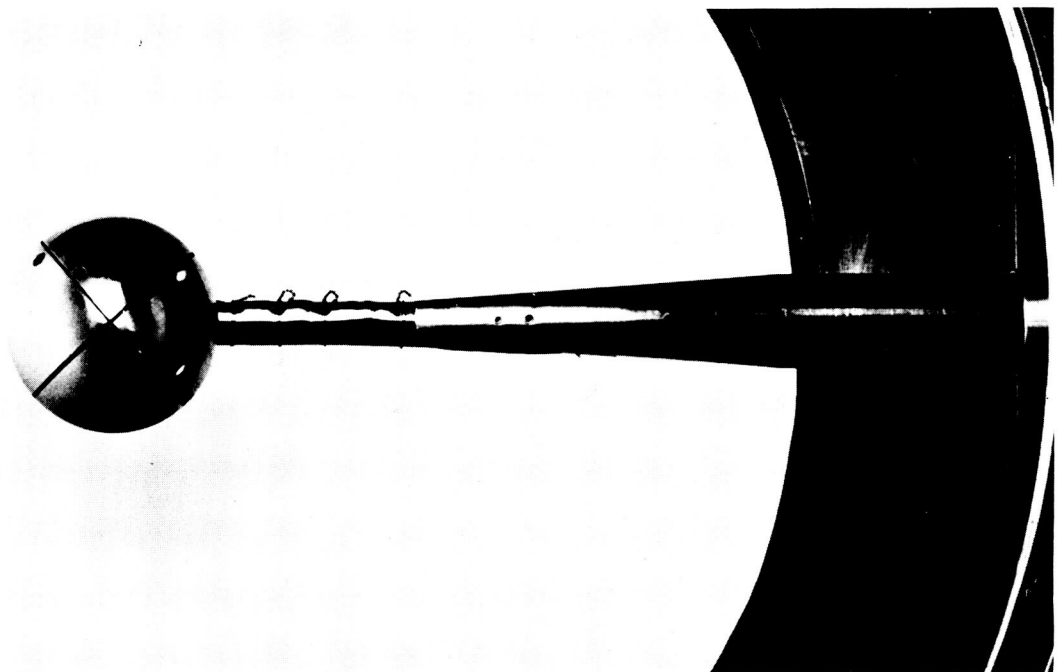


Fig. 14. Calibration sphere on sting-support gas bearing

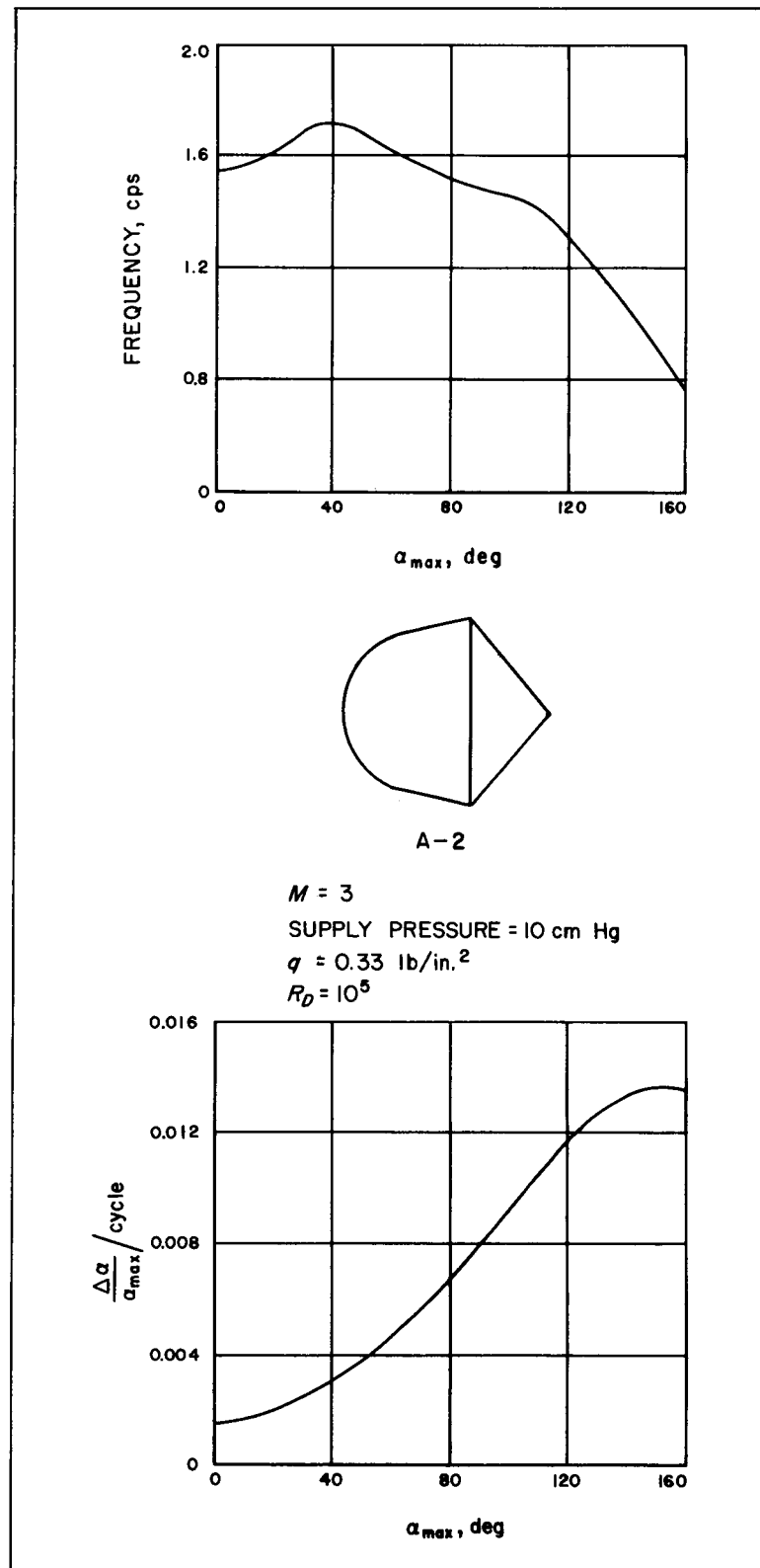
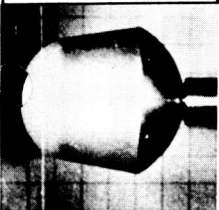
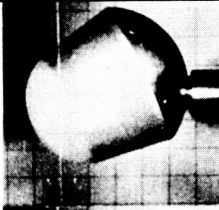
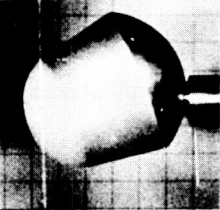
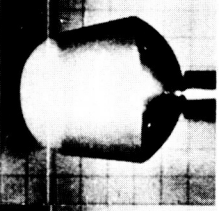
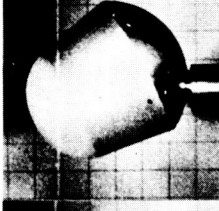
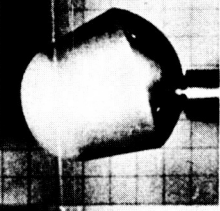
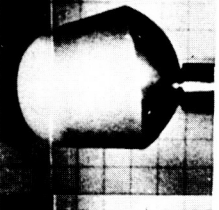
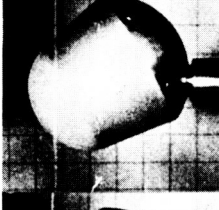
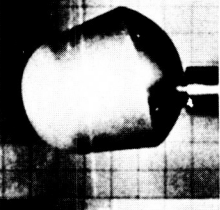
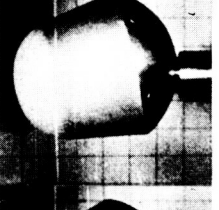
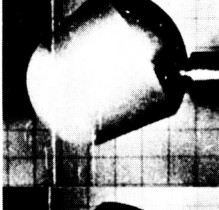
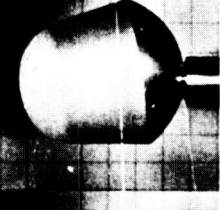
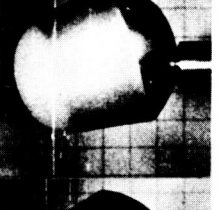
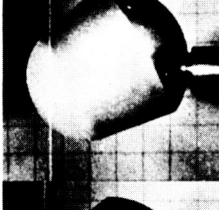
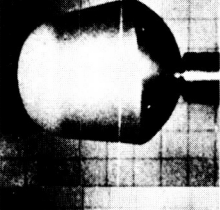
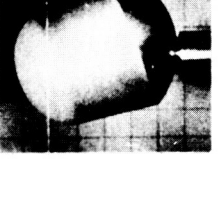
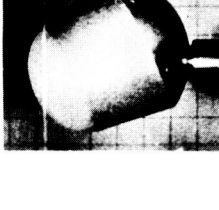
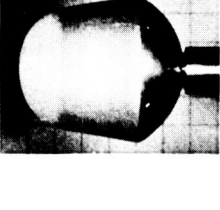


Fig. 15. Typical cross-support gas-bearing model damping data as recorded by the internal angle-of-attack readout system

	α , deg	TIME sec		α , deg	TIME sec		α , deg	TIME sec
	+1.3	0.571		-25.3	0.625		-22.8	0.675
	-3.6	0.580		-28.2	0.633		-18.9	0.682
	-8.4	0.589		-30.1	0.642		-14.6	0.690
	-13.0	0.598		-30.0	0.650		-9.9	0.697
	-17.4	0.607		-28.5	0.658		-5.1	0.704
	-21.6	0.616		-26.1	0.667		0	0.710

$M = 6$, SUPPLY PRESSURE = 530 cm Hg, $R_D = 5.6 \times 10^5$, 0.85 in. GRID SPACINGS, MODEL DIAMETER 3.6 in.

Fig. 16a. 16-mm motion pictures showing one-half cycle of oscillatory motion of A-5 model on sting-support gas bearing in hypersonic wind tunnel

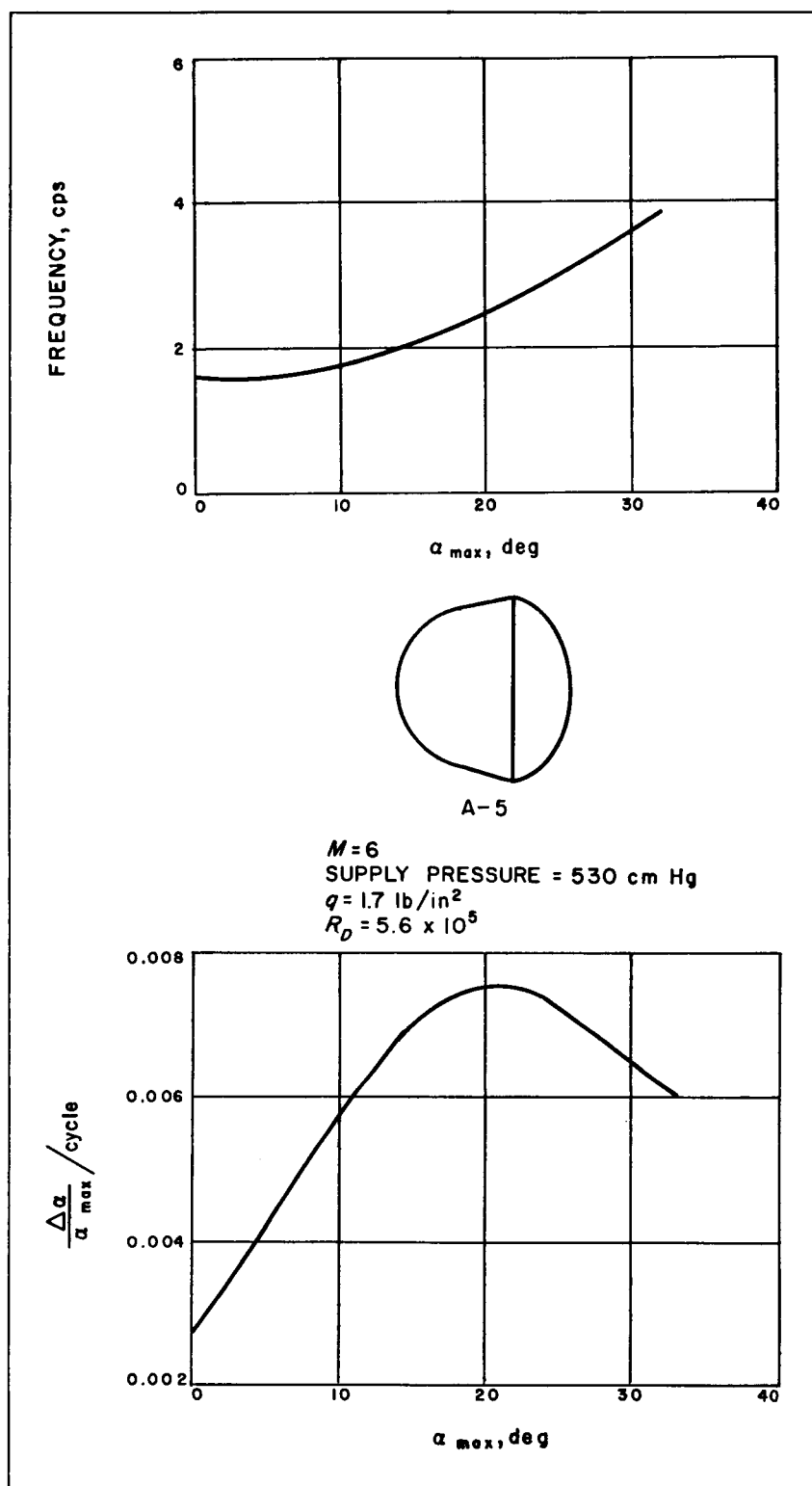


Fig. 16b. Typical sting-support gas-bearing model damping data as read from 16-mm motion picture film

IV. CAPTIVE-MODEL DATA REDUCTION

A. Equation of Motion

The decision to use the captive, high-amplitude, free-oscillation technique for determining pitch damping made it necessary to understand the data reduction and subsequent data application problems. The single-degree-of-freedom equation of motion for a body oscillating about a fixed axis, such as models supported in a wind tunnel on a gas bearing, is

$$I\ddot{\alpha} + M_D\dot{\alpha} + M = 0 \quad (6)$$

In the general case, I is constant, but M_D and M are functions of α . In the simple linear case, M_D is constant, and M is linear with α ; i.e.,

$$M = M_\alpha \alpha \quad (7)$$

For the usual case of an aerodynamic shape,

$$\left(\frac{M_D}{2I}\right)^2 \ll \frac{M_\alpha}{I} \quad (8)$$

Therefore, the approximate solution to Eq. (6) is in the form:

$$f = \frac{1}{2\pi} \left(\frac{M_\alpha}{I} \right)^{\frac{1}{2}} \quad (9)$$

$$\frac{\alpha}{\alpha_0} = \exp \left(- \frac{M_D}{2I} t \right) \cos(\omega t) \quad (10)$$

For the more general nonlinear case, in order to demonstrate the effects of pitching moment and pitch damping upon the motion of a model mounted on a gas bearing, Eq. (6) was solved numerically on an IBM 7090 computer for several assumed-typical combination values of M_D/I and M/I expected for very short, high-drag bodies of revolution. For the purposes of this Report, discussion will be limited to the case shown in Fig. 17 since its results are typical.

$$C_m = -0.2 \sin \alpha \quad (11)$$

$$(C_{m_q} + C_{m_{\dot{\alpha}}}) = -0.05 \left(1 + \frac{2}{90} |\alpha \text{ deg}| \right) \quad (12)$$

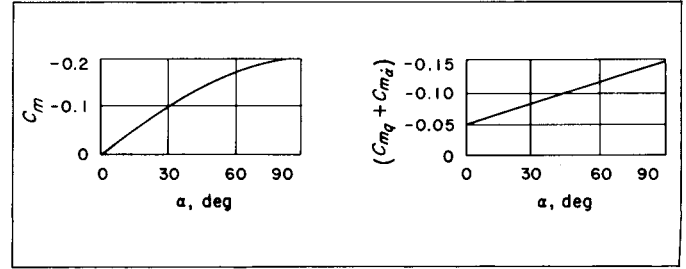


Fig. 17. Analytical example of local pitching moment and pitch damping

where

Mach number = 2

free-stream dynamic pressure, $q = 5 \text{ lb/in.}^2$

free-stream velocity, $V = 1750 \text{ ft/sec} = 21,000 \text{ in./sec}$

model moment of inertia, $I = 0.01 \text{ in. lb sec}^2$; (equivalent to a 4-in. D sphere with a 0.1-in.-thick steel shell)

$A =$ model reference area ($\pi d^2/4$) = 12.56 in.^2

$d =$ model reference length (D) = 4 in.

$$\frac{M_D}{I} = \frac{qAd^2}{VI} (C_{m_q} + C_{m_{\dot{\alpha}}}) = 0.24 \left(1 + \frac{2}{90} |\alpha \text{ deg}| \right) \quad (13)$$

$$\frac{M}{I} = \frac{qAdC_m}{I} = 5028 \sin \alpha \quad (14)$$

The solution of Eq. (6) for the equations stated above gives an oscillation frequency and a rate of angle-of-attack decay as a function of the amplitude of the angle-of-attack oscillation as shown in Fig. 18. The term $\Delta\alpha/\alpha_{\max}$ is defined in Fig. 19. If the pitching-moment slope and pitch-damping values of the sample case did not vary with α , the solution of Eq. (6), indicated in Fig. 18, would have constant values of frequency and $\Delta\alpha/\alpha_{\max}$ equal to the values at $\alpha_{\max} = 0$. The divergence from constant values of frequency and $\Delta\alpha/\alpha_{\max}$ in Fig. 18 indicates the effect of realistic aerodynamic coefficients upon the solution of the equation of motion [Eq. (6)] relative to the linear solution.

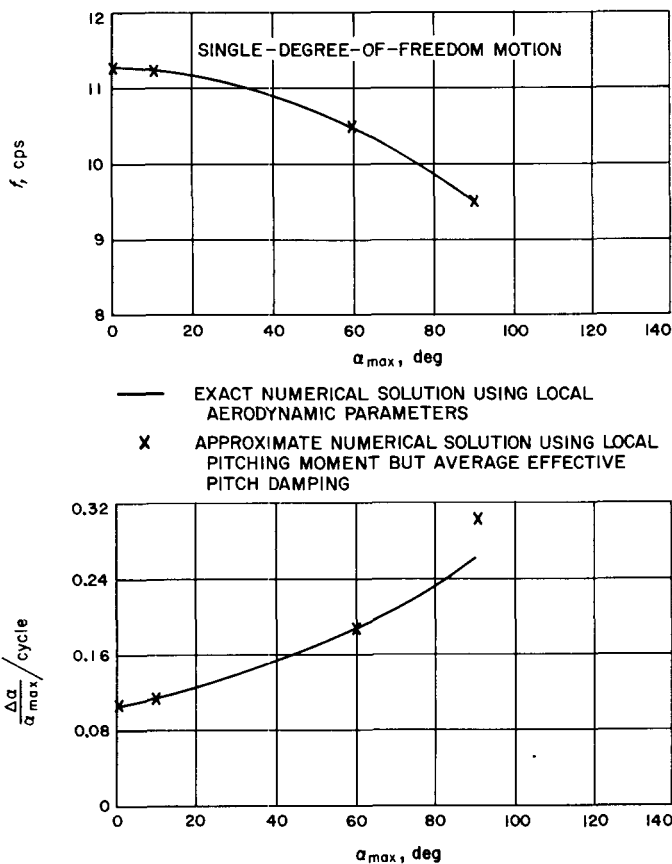


Fig. 18. Analytical study of aerodynamic pitch damping

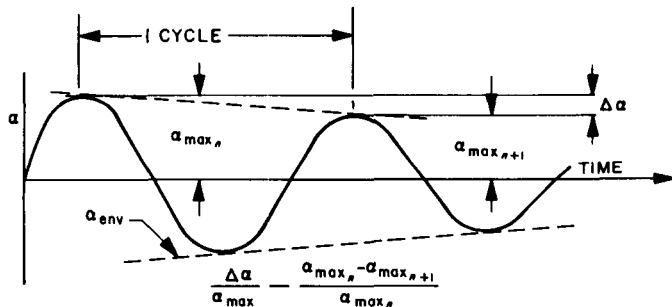


Fig. 19. Definition of the amplitude rate of decay

B. Data Reduction

Several approaches can be used to determine the pitch damping from the oscillatory history of a model oscillating freely on a gas bearing. The suggested basis for these approaches is the use of the amplitude-decay-rate per cycle and the frequency as functions of the oscillation envelope. The most elegant procedure would yield the exact pitch-damping values as a function of the local angle of attack. The simplest approach would be to take the values of the amplitude-decay-rate per cycle and the

frequency at each particular amplitude of oscillation and solve for the pitch damping (as a function of the amplitude of oscillation) using the simplified linear solution to Eq. (6):

$$M_D = -2If \ln(1 - \Delta\alpha/\alpha_{\max}) \quad (15)$$

A compromise approach would be to solve Eq. (6) for the motion of the model using the actual pitching-moment curve as a function of the local angle of attack, and to determine the proper value of pitch damping which would remain constant during an entire cycle of oscillation and would be a function of that particular oscillation amplitude. A brief discussion of each of these techniques would serve to acquaint the reader with the problems, and the advantages and disadvantages of each approach. Analysis on the reduction of actual flight vehicle-entry data is reported in Ref. 13.

1. Complete, Exact Solution

Given the frequency and amplitude decay rate for the oscillation envelope from 0 to 90 deg of Fig. 18, in principle it is possible to determine M and M_D as local functions of α for $0 \text{ deg} < \alpha < 90 \text{ deg}$. In practice, although M is easily determined to a high degree of accuracy, the accuracy of M_D falls off rapidly at $\alpha > 40 \text{ deg}$, even by the use of a complex program on a large high-speed digital computer. This is to be expected as $M \gg M_D \dot{\alpha}$ for α near α_{\max} since $\dot{\alpha}$ approaches zero. Therefore, in order to obtain local values of M_D up to some desired α , it is necessary to have the data (frequency and decay rate) from $\alpha_{\max} = 0$ to an α_{\max} considerably greater (say a factor of 2) than the α to which the local damping data are desired.

The exact solution for M_D from Eq. (6), using the frequency and decay curves of Fig. 18, is quite good for local angles of attack up to about 40 deg. However, the solution for M_D begins to fall off rapidly for larger α , and by $\alpha = 90 \text{ deg}$, no meaningful solution for M_D exists. On the other hand, as the values of M_D at α 's approaching α_{\max} have small effect on the decay in that α_{\max} oscillatory amplitude, there may be no real need to determine M_D to a high degree of accuracy at local angles of attack near the expected maximum angle of oscillation.

2. Simplest Solution

For the reduction of the single-degree-of-freedom motion data taken with the gas bearing, the values of $\Delta\alpha/\alpha_{\max}$ and the frequency at each particular α_{\max} were used to determine an effective average value of M_D , which can be

nondimensionalized to $(C_{m_q} + C_{m_{\dot{\alpha}}})$ by using the simplified linear solution to Eq. (6) which results in Eq. (15). For the example in Section IV A, the validity of using the average effective pitch damping was investigated analytically. Equation (15) was used to obtain average effective pitch damping at α_{\max} near 0 deg, and at 10, 60, and 90 deg from the oscillation frequency and decay curves in Fig. 18. That is, the value of f and $\Delta\alpha/\alpha_{\max}$ at a particular α_{\max} substituted into Eq. (15) yielded an average effective pitch damping for that α_{\max} . In turn, at each particular α_{\max} , the corresponding value of average effective damping (assumed to be constant throughout an entire cycle of oscillation) was put back into Eq. (6) along with the exact local angle-of-attack pitching moment ($C_m = -0.2 \sin \alpha$) in order to obtain the amount of amplitude decay over one cycle of oscillation. The resulting $\Delta\alpha/\alpha_{\max}$ vs α_{\max} values for this average effective pitch-damping approach compare quite favorably with the exact nonlinear solution. The comparisons are indicated in Table 2, as well as shown in Fig. 18. The maximum discrepancy occurs at $\alpha_{\max} = 90$ deg, is only 15% in $\Delta\alpha/\alpha_{\max}$, and decreases to a negligible 2% by $\alpha_{\max} = 60$ deg. This same procedure was applied to a number of typical values of M_D/I and M/I vs α , resulting in similar good comparisons with the exact case; i.e., well within 10% for $\alpha_{\max} \leq 60$ deg.

3. Compromise Solution

The error in the determination of an average effective pitch-damping value incurred by use of the simplest solution is the result of using an effective constant pitching-moment slope. In order to eliminate the slight detrimental effect of this effective constant-pitching-moment slope assumption and still avoid the difficult procedure for determining local angle-of-attack values of the pitch damping, a compromise approach is suggested. Equation (6) can be solved at specific amplitudes of oscillation for an average effective value of pitch damping at each α_{\max} with the use of an exact pitching moment curve.

Table 2. Comparison of effective average solution of oscillation amplitude decay with the exact solution

α_{\max} , deg	M_D/I		$\Delta\alpha/\alpha_{\max}$ per cycle		Discrepancy in $\Delta\alpha/\alpha_{\max}$, %
	Exact local value	Average effective value, constant over 1 cycle	Exact solution	Effective average solution	
≈ 0	0.24 (1 + 2/90 α deg)	0.2400	0.0105	0.0105	0
10		0.2622	0.0116	0.0117	1
60		0.3934	0.0186	0.0190	2
90		0.5071	0.0261	0.0300	15

The pitching-moment curve can be experimentally determined from a static stability test, or an approximate calculation using, for example, the Newtonian flow assumption, or calculated from an experimentally determined spectrum of frequency vs amplitude of oscillation.

This procedure is the most realistic approach, as it parallels a practical procedure for determining the trajectory motion of an entry vehicle by using the six-degree-of-freedom equations. However, the added complication of this method over the simplest approach (Section IV. B. 2.) does not appear justified for the general case of determining average effective pitch damping. Because of the simplicity of using Eq. (15) and the resulting insignificant error in the determination of the pitch damping in the range of amplitudes ($\alpha_{\max} < 60$ deg) required for the six-degree-of-freedom equations-of-motion entry studies, the simplest approach (Section IV. B. 2.) was the method used to reduce the data in this Report.

V. FREE FLIGHT

Simplified free-flight testing in a conventional wind tunnel (Ref. 14) can be useful for obtaining pitch damping of models at large angles of oscillation. Preliminary work has been done with a model of shape A-1. The testing technique consists of taking high speed motion pictures (35-mm film, 4500 frames/sec) of models in flight across the wind-tunnel viewing windows. These models⁴ are suspended at the desired maximum oscillation angle on a 0.020-in.-D vertical wire located at the leading edge of the windows, and are released by breaking the wire at a notch within the model when an impulse load is added to the wire's tension load. The oscillatory motion is generally confined to the vertical plane, thus giving three-degree-of-freedom motion.

Preliminary data taken of the aforementioned model shape in both the JPL 20-in. supersonic and 21-in. hypersonic wind tunnels (Ref. 15) are shown in Figs. 20 and 21. Although the data from each frame are plotted, for brevity, only pictures from every other frame are shown. The motion is documented throughout the flight by closely spaced (both in time and angle of attack) pictures. The relative flatness of the base of these models in flight indicates that the oscillatory motion was virtually confined to the vertical plane. The base bulge can be measured in order to estimate any angle of yaw. Otherwise, mirrors could be placed inside the test section at 45-deg angles to the test section floor and ceiling, and parallel to the airflow. In this manner, each frame of the single roll of motion picture film will record the model-motion data in the two streamwise orthogonal planes. The accuracy to which the model angles of attack can be read is demonstrated in the graphs of Figs. 20 and 21. Figure 22 contains enlargements of the models in flight, and in spite of the film grain and light diffraction problems, the reading repeatability is to the nearest $\frac{1}{2}$ deg. However, until a substantial variety of models have been tested on the gas bearing and in free-flight through a large range of conditions, no definite conclusions can be made about the accuracy and repeatability to which pitch-damping data can be measured.

Additional consideration should be given to the wide ranges of variables possible with the free-flight technique in studying model oscillatory motion. The tunnel operating range at any Mach number can be varied by

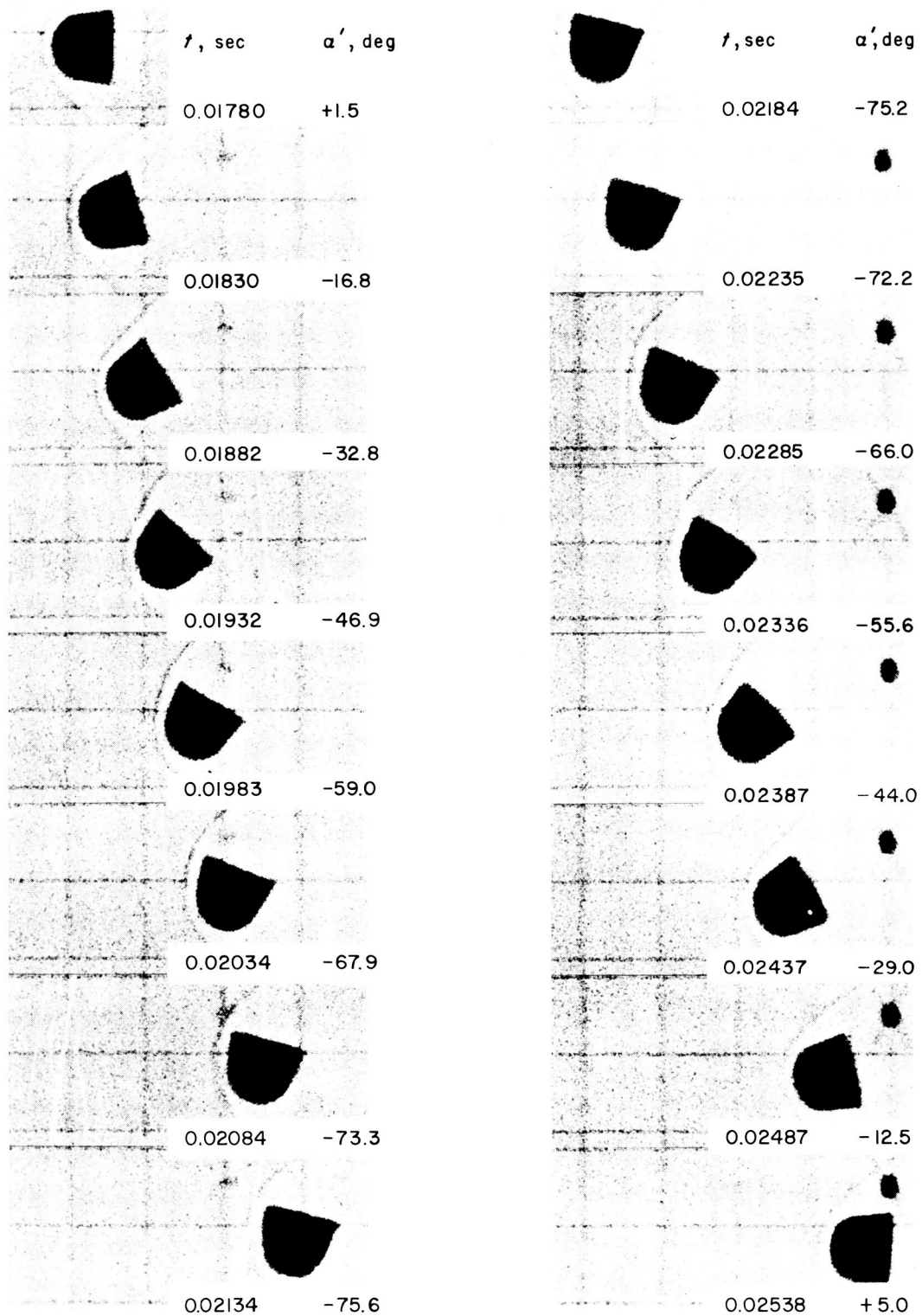
one order of magnitude and, for a given model size and weight, the moment of inertia can also be varied by one order of magnitude. The ballistic coefficient $m/C_D A$ can be varied through two orders of magnitude. These variations make it practical to duplicate or simulate certain characteristics of the flight vehicle's expected motion during an atmosphere entry trajectory. Not all the important characteristics can be simulated, and, of those that can be, it may be necessary to do one at a time. In any case, sufficient variation of the testing parameters can be made in order to verify the experimentally determined aerodynamic parameters and obtain a better insight into the vehicle motion as determined by the use of the six-degree-of-freedom equations of motion.

For example, it is possible to design a model and pick a wind-tunnel operating condition in order to duplicate the degradation of the dynamic pressure per cycle of oscillation expected for the flight vehicle during an atmosphere entry trajectory after the region of maximum deceleration.⁵ Also, in many cases it is possible to match the dimensionless oscillatory frequency (Strouhal number) during a trajectory by choosing the proper model moment of inertia and/or wind-tunnel operating condition. In certain instances, the expected Reynolds number of an actual entry vehicle can be matched. For the full-scale characteristics which cannot be duplicated or simulated, it is practical to vary the mismatch in the scaling of the model test conditions through a very large range, and consequently make it possible to better evaluate the validity of applying the model data to the expected flight condition.

There is no need or justification to rely solely upon the use of limited experimental data (which at times may be questionable) in six-degree-of-freedom equation-of-motion studies in order to estimate the expected motion of a vehicle during entry into an atmosphere. The data obtained from one set of model test conditions can be used to compare with the motion of other widely different model test conditions as predicted by the six-degree-of-freedom program. In this way, confidence in (or limitations of) the use of the six-degree-of-freedom motion studies can be established.

⁴The 1-in.-D models were cast from light-weight polyurethane foam (averaging about 6 lb/ft³), and each was ballasted with a 0.45-in.-D lead sphere.

⁵The per-cycle dynamic pressure degradation for the free-flight cases shown in Figs. 20 and 21, are about the same as was estimated for the atmosphere entry case in Fig. 2 at the corresponding Mach numbers, but for an initial entry angle of 40° rather than the 90° case shown.



$M = 3$, SUPPLY PRESSURE = 80 cm Hg, $R_D = 2.0 \times 10^5$, 1-in. GRID SPACINGS

Fig. 20a. High speed motion pictures showing A-1 model during one-half cycle of flight in supersonic wind tunnel

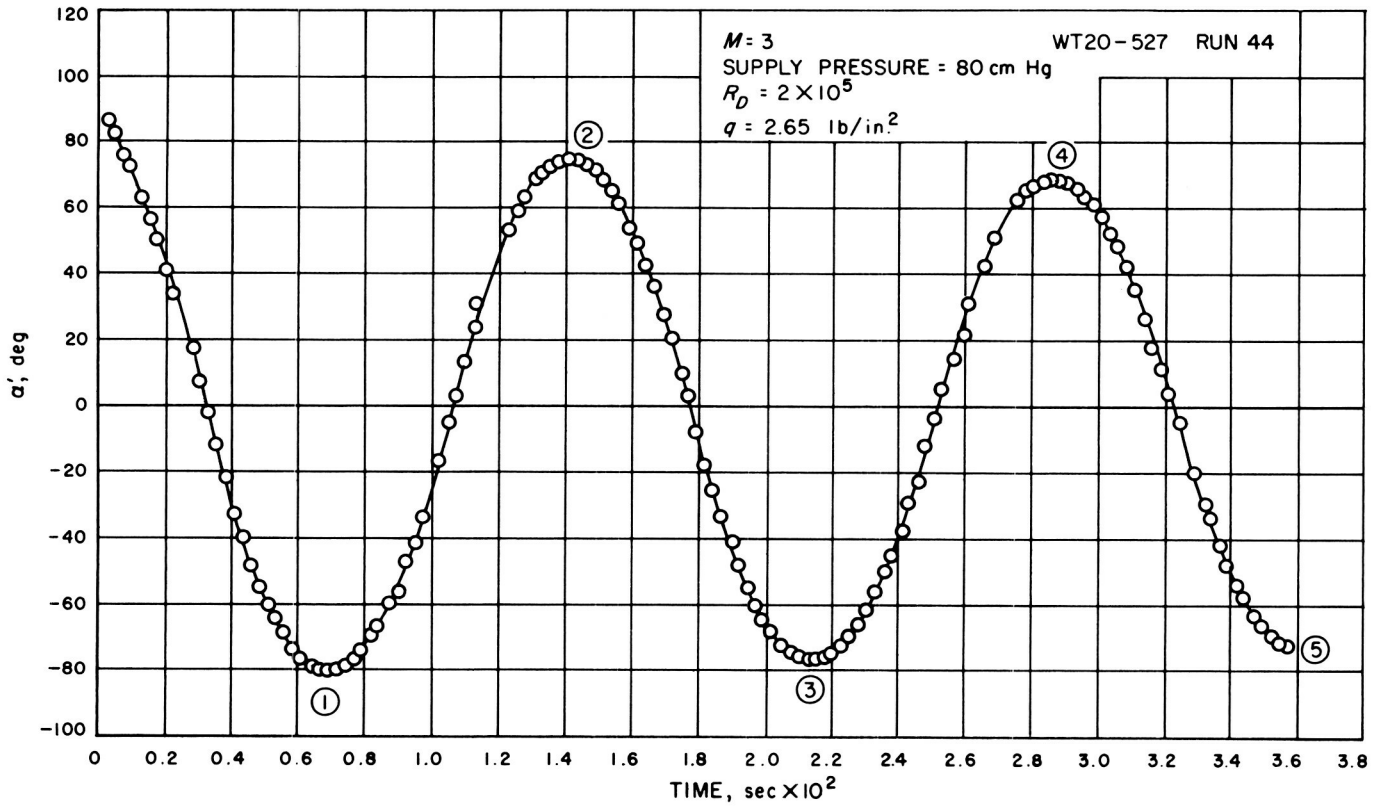
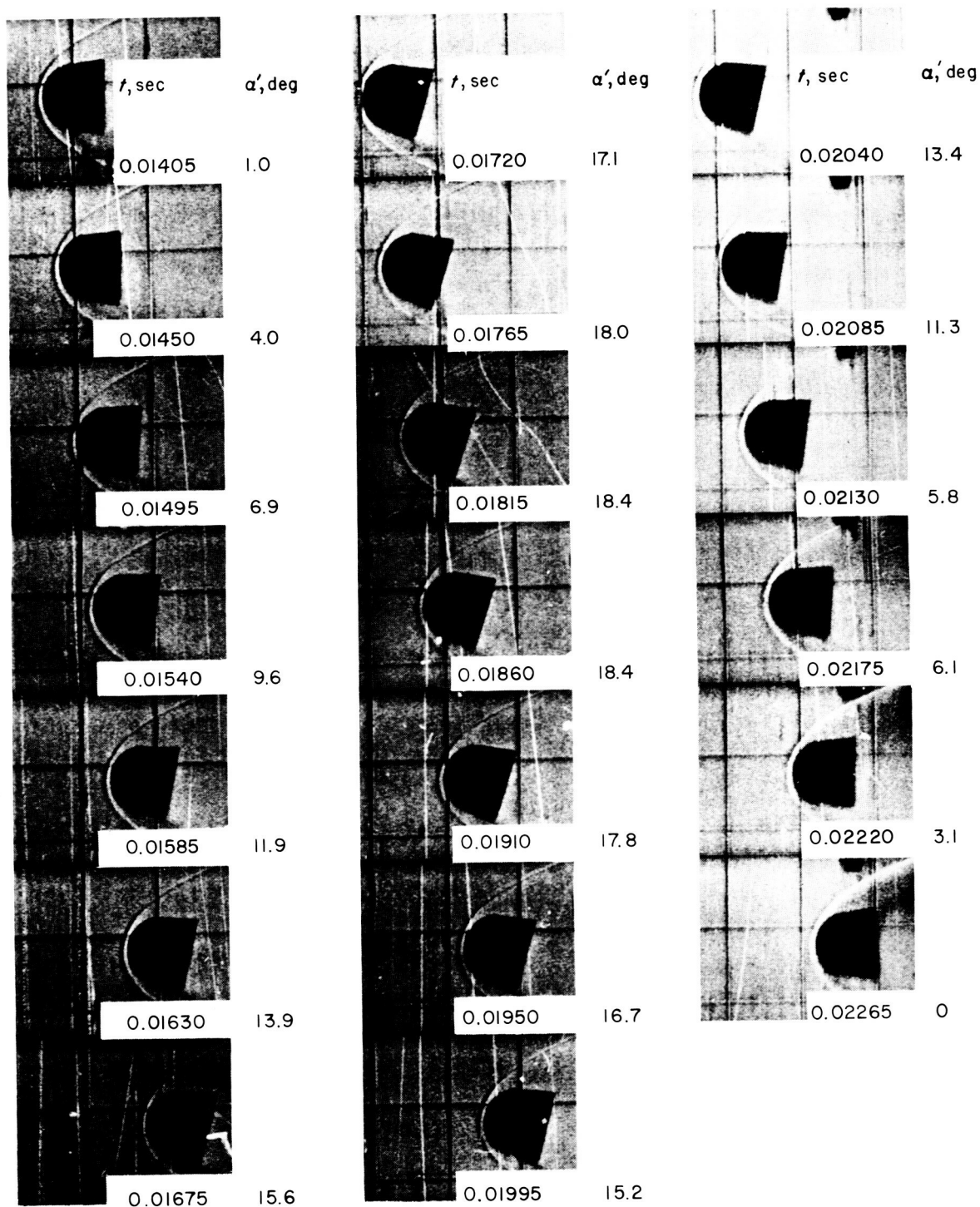


Fig. 20b. Angle of attack vs time, A-1 free-flight model (supersonic wind tunnel)



$M=7.3$, SUPPLY PRESSURE = 2000 cm Hg, $R_D = 2.6 \times 10^5$, 1-in. GRID SPACINGS

Fig. 21a. High speed motion pictures showing A-1 model during one-half cycle of flight in hypersonic wind tunnel

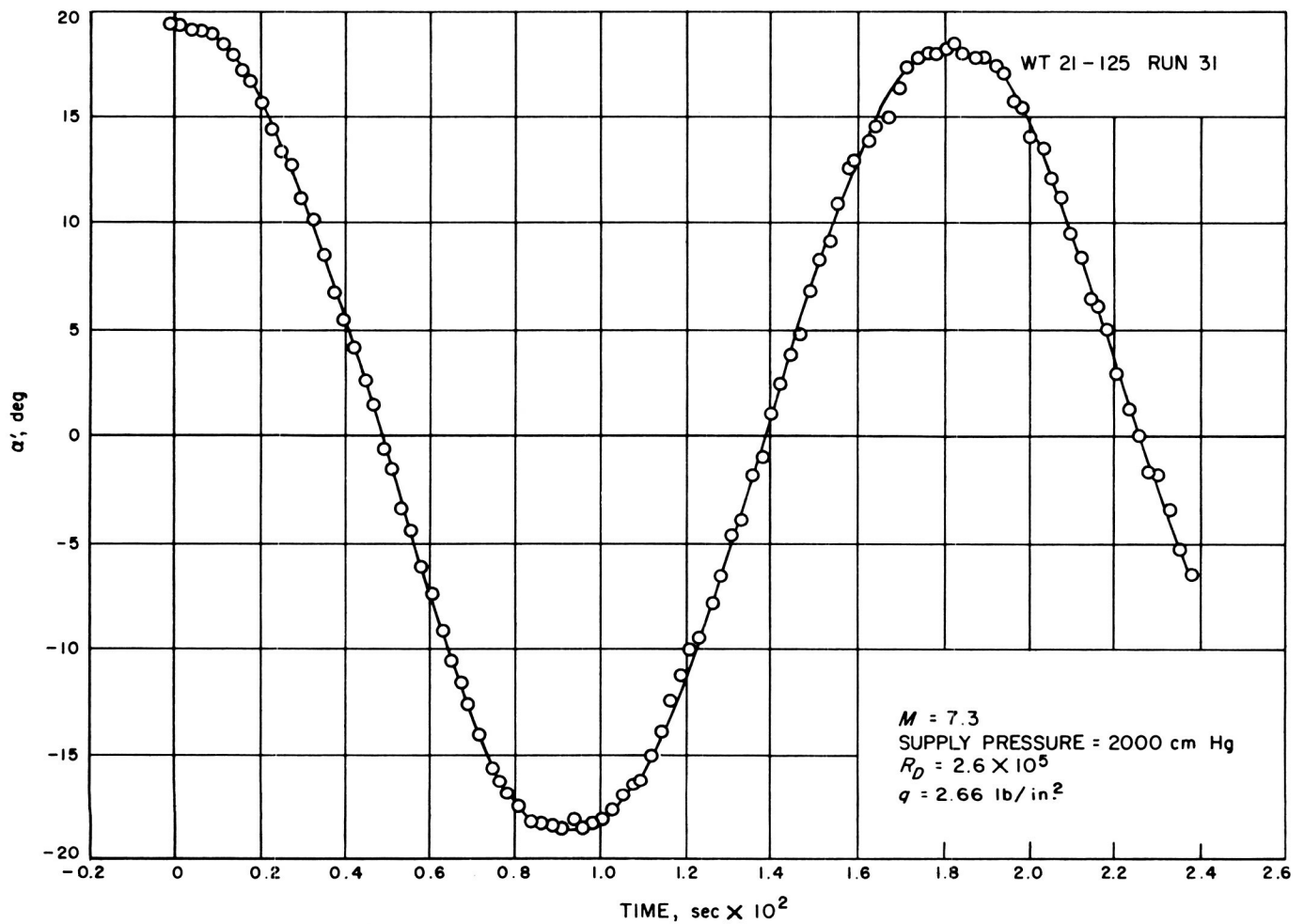
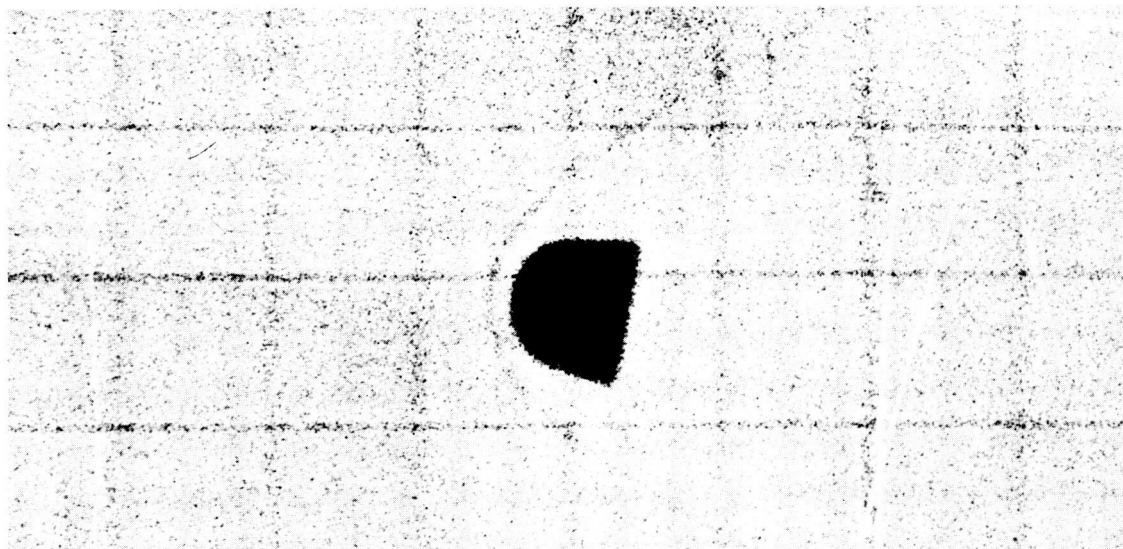
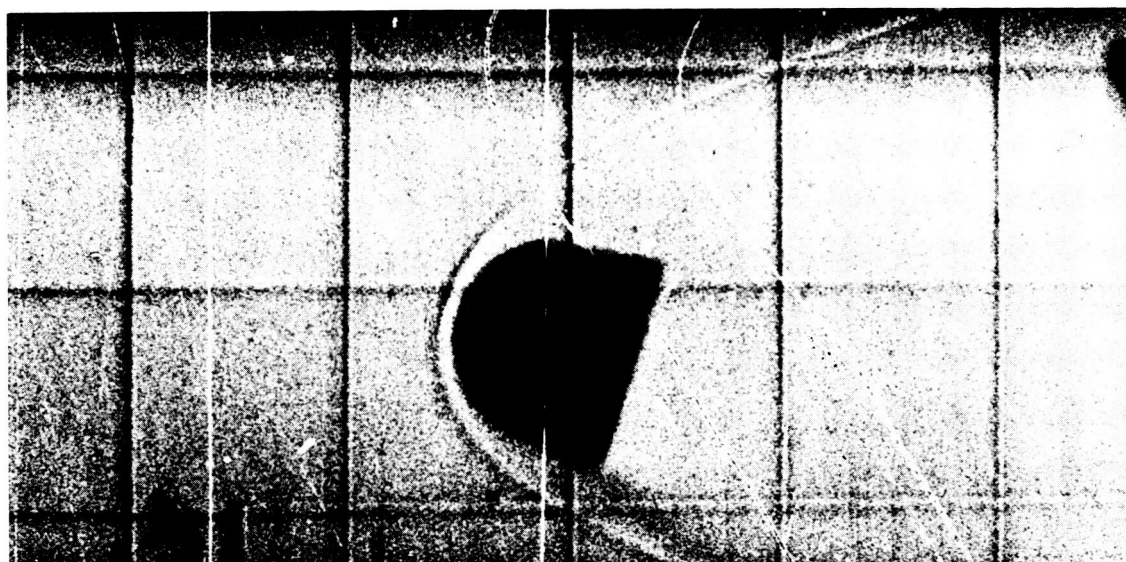


Fig. 21b. Angle of attack vs time, A-1 free-flight model (hypersonic wind tunnel)



SUPERSONIC WIND TUNNEL
SUPER HYPAN ASA 500
f5.6 4000 frames/sec
IMAGE SIZE ON FILM: 0.032-in. BASE DIAMETER



HYPERSONIC WIND TUNNEL
TRI-X ASA 320
f5.6 4500 frames/sec
IMAGE SIZE ON FILM: 0.096-in. BASE DIAMETER

Fig. 22. Enlargement of sample 35-mm half-frame pictures of A-1 model in flight

VI. TYPICAL EXPERIMENTAL RESULTS⁶

For purposes of illustration, results typical of the data (Ref. 16) obtained are included.⁷ The model center-of-gravity location for these captive tests, as well as for the free-flight examples, appears in Table 3. Figure 23 is a composite of model pitch-damping data obtained on the gas bearing through the Mach number range. As all of the data obtained with the sting-supported gas bearing (shape A-5), for the testing conditions covered ($2 < M < 6$ and $0.4 < q < 3 \text{ lb/in.}^2$), fall within the shaded region, there did not seem to be any need for further defining the data for this Report. The average effective pitch damping increases with increasing angle of oscillation and decreases with increasing Mach number. The $M = 4\frac{1}{2}$ curve is at a substantially different level than the $M = 3$ curve, but it does compare quite favorably with the $M = 6$ curve. The repeatability of the $(C_{m_q} + C_{m_{\dot{\alpha}}})_{\text{avg}}$ data obtained is generally within ± 0.01 .

Included in Fig. 23 is the pitch-damping coefficient from the free-flight case of Fig. 20. As the model base configurations are considerably different, additional data are necessary before any definite conclusions can be reached. Direct comparison of Fig. 20 with Fig. 24 will not yield the $(C_{m_q} + C_{m_{\dot{\alpha}}})_{\text{avg}}$ value of the free-flight data point appearing in Fig. 23, for two reasons. The actual free-flight model did have some yawing motion (Table 4), which was used to correct the vertical plane angle angle-of-attack data shown in Fig. 20. Also, "subjective"

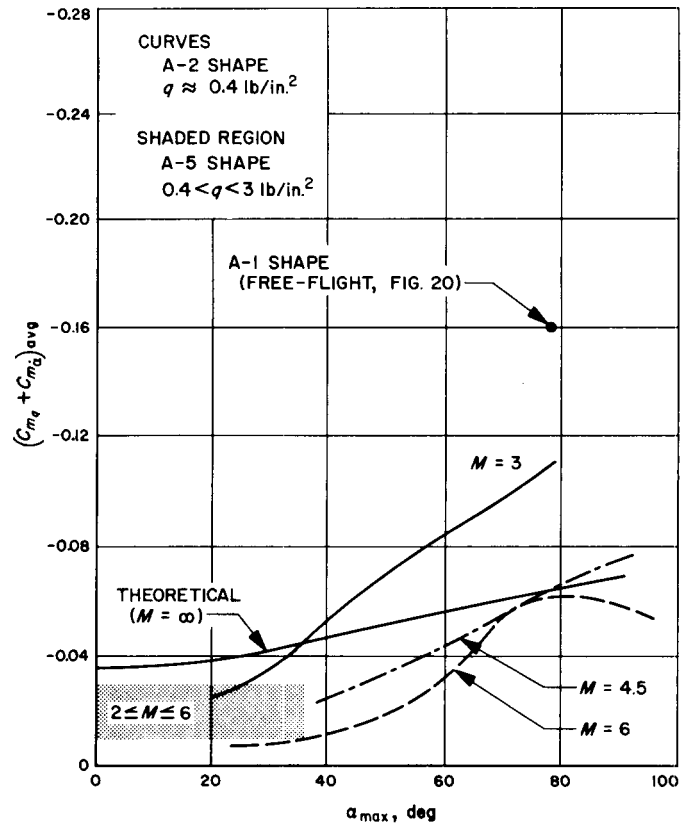


Fig. 23. Average effective pitch damping vs oscillation amplitude

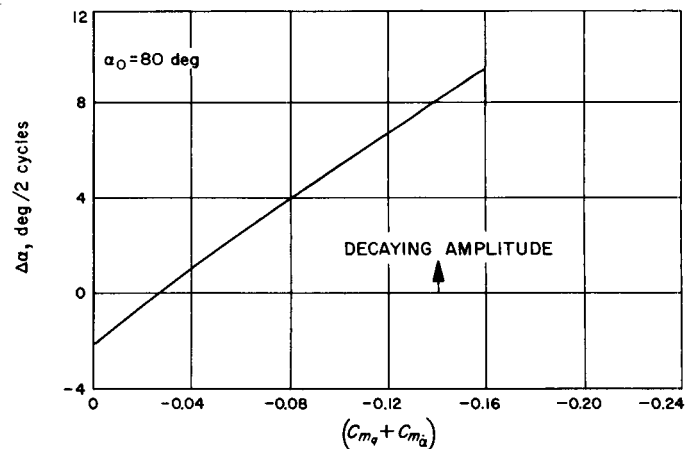


Fig. 24. Six-degree-of-freedom data reduction for free flight trajectory of Fig. 20

⁶ See Table 3 for center-of-gravity locations.

⁷ Reference 17 contains a great deal of pitch damping data ($2 < M < 9$, for models similar to shape P, obtained by use of the sting-supported gas bearing. The reader may consult this reference for an additional example of an extensive program of blunt-body pitch damping testing with a gas bearing. Pitch damping data were obtained for the model rotation axis off as well as on the plane of symmetry.

Table 3. Location of center of gravity (experimental) for pitch-damping measurements

Shape	cg location (d from nose)
A-1	0.449
A-2	0.482
A-5	0.528
B-2	0.414

judgment was used in interpreting the decay rates (Table 5) of the unsymmetrical oscillatory motion shown in Fig. 20.

Table 4. Corrected amplitudes
(Fig. 20)

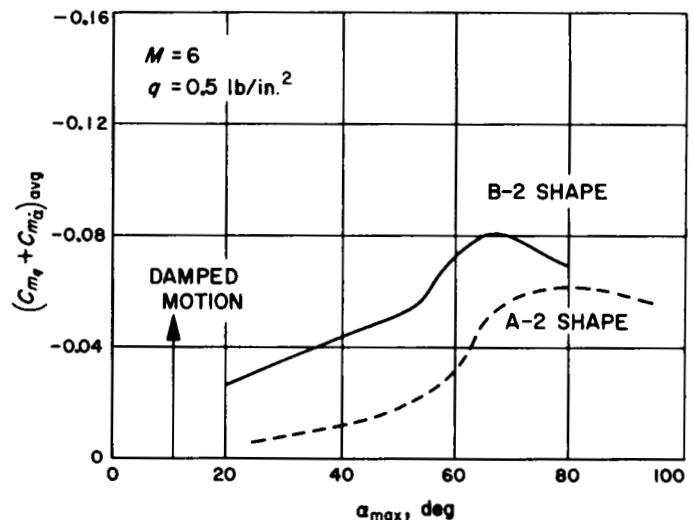
Peak	Time, sec	α' , deg	ψ'_B , deg	α , deg
1	0.00695	79.5	0	79.5
2	0.01420	74.3	0	74.3
3	0.02150	76.0	0	76.0
4	0.02885	68.0	9	68.3
5	0.03610	72.0	17	72.8
$\cos \alpha = \cos \alpha' \cos \psi'_B$				

Table 5. Amplitude decay rates
(Fig. 20)

Peaks	α_{\max} , deg	$\Delta\alpha$, deg	$\Delta\alpha/\alpha_{\max}$
1-3	79.5	3.5	.0440
3-5	76.0	3.2	.0421
2-4	74.3	6.0	.0808

This free-flight point was computed by use of the same six-degree-of-freedom equations of motion used to calculate the entry trajectories discussed in Section II. Certain alterations were required in order to adapt this general program to the specific case of a wind tunnel free-flight trajectory. The calculation procedure followed was to use known static values for the aerodynamic parameters of lift, drag, and pitching moment along with the proper model mass characteristics and model attitude and velocity. Then, by interpolation from several calculations using various values of $(C_{m_q} + C_{m_{\dot{\alpha}}})$, a value of $(C_{m_q} + C_{m_{\dot{\alpha}}})$ was determined that would give a calculated amplitude decay equal to that experimentally observed. The results of such six-degree-of-freedom calculations appear in Fig. 24. In order to show the over-all sensitivity for determining $(C_{m_q} + C_{m_{\dot{\alpha}}})$ from the amplitude decay, the amplitude decay is given in degrees per two cycles of motion as a function of $(C_{m_q} + C_{m_{\dot{\alpha}}})$. One degree amplitude variation is equivalent to about 0.014 in $(C_{m_q} + C_{m_{\dot{\alpha}}})$. This sensitivity is adequate for the accuracy required in $(C_{m_q} + C_{m_{\dot{\alpha}}})$ as shown by the effect of $(C_{m_q} + C_{m_{\dot{\alpha}}})$ in Fig. 8, and is compatible to the accuracy with which the oscillation amplitudes of the free-flight model can be read from the high-speed motion-picture film.

Also shown in Fig. 23 is a theoretical average effective damping as a function of the amplitude of oscillation for the A-2 shape. Simple, unmodified, Newtonian theory was used to obtain this damping as a function of the

**Fig. 25. Average effective pitch damping vs oscillation amplitude, cross-support gas bearing**

local angle of attack and these results in turn were integrated to yield the average effective damping as a function of α_{\max} . This analytical approach is applicable only for $M > 4$. The comparison of this analytical damping with the experimental damping at the higher angles of oscillation is quite good.

In Fig. 25, the cross-support gas-bearing pitch damping at $M = 6$ for the A-2 shape is compared with that of a somewhat blunter shape, the B-2. These preliminary data indicate a somewhat greater pitch damping for the more blunt shape. It will be very fortuitous if this result is confirmed in tests already being readied, as the more blunt B-2 shape would require the existence of more pitch damping to prevent divergence in oscillatory motion at the $M = 3$ region than the A-2 shape (see Fig. 9).

Mach = 3 data were recorded for both a cross-support ball-bearing and a gas-bearing mount for the A-2 model. The reduced data (which have been corrected for the bearing friction) from these two approaches actually compare quite favorably. In Fig. 26, the relative bearing damping is shown in order to demonstrate the need for a low-friction bearing. The ball-bearing-mount curve was terminated when the magnitudes of the aerodynamic and bearing friction damping were the same, because the accuracy of the ball-bearing damping is uncertain to within a factor of two. However, the accuracy of the gas-bearing damping appears to be well within a factor of two, and this friction damping is generally small relative to the small aerodynamic damping measured.

The range of gas-bearing damping (as measured with a sphere mounted on an axis through its center) for the

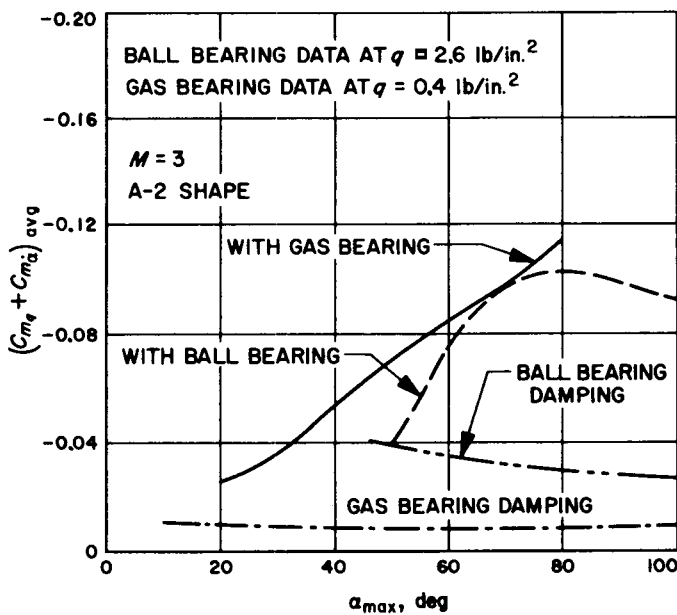


Fig. 26. Comparison of average effective pitch-damping gas bearing vs ball bearing

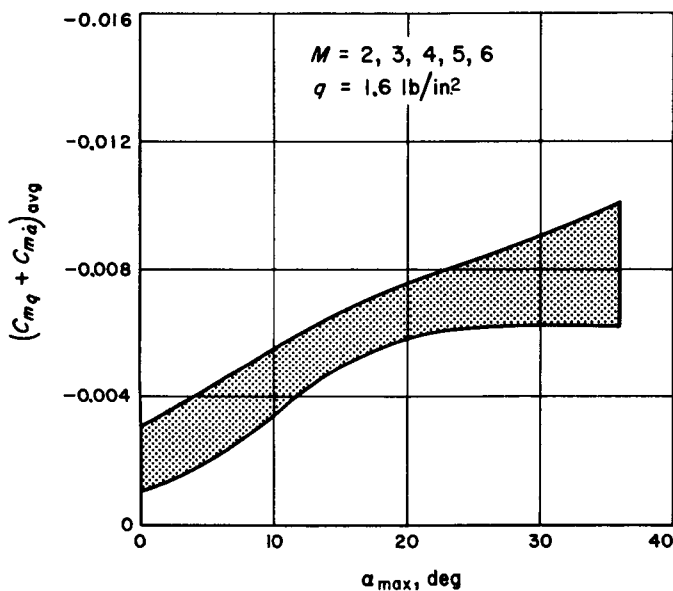


Fig. 27. Sting-support gas-bearing damping as measured with a calibration sphere, at various Mach numbers

sting-supported model (Fig. 14) is shown in Fig. 27 for $2 < M < 6$ at a tunnel dynamic pressure of 1.6 lb/in^2 . The level of the tare damping is small in comparison with the aerodynamic damping and is essentially independent of Mach number. The tare damping measured with a "calibration" sphere is caused by the sphere-surface skin

friction, the gas-bearing friction, and the aerodynamic damping of the slot in the base of a sting-mounted sphere. Although the surface skin friction is small relative to the bearing friction, it is suspected that the aerodynamic damping of the slot may be substantial. This is demonstrated by the damping curves in Fig. 28 for both the sting-supported and cross-supported gas bearings. Although the two systems appear to have about the same damping near zero amplitude of oscillation, the sting-mounted-system damping increases with amplitude of

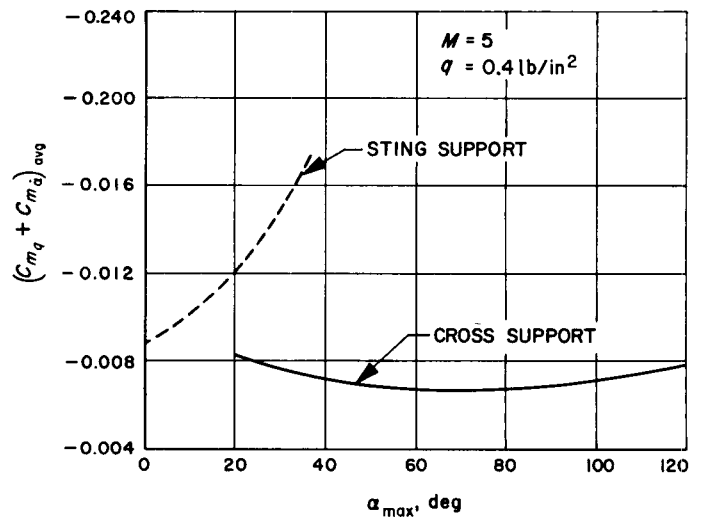


Fig. 28. Comparison of gas-bearing damping (sting vs cross support) as measured with a calibration sphere

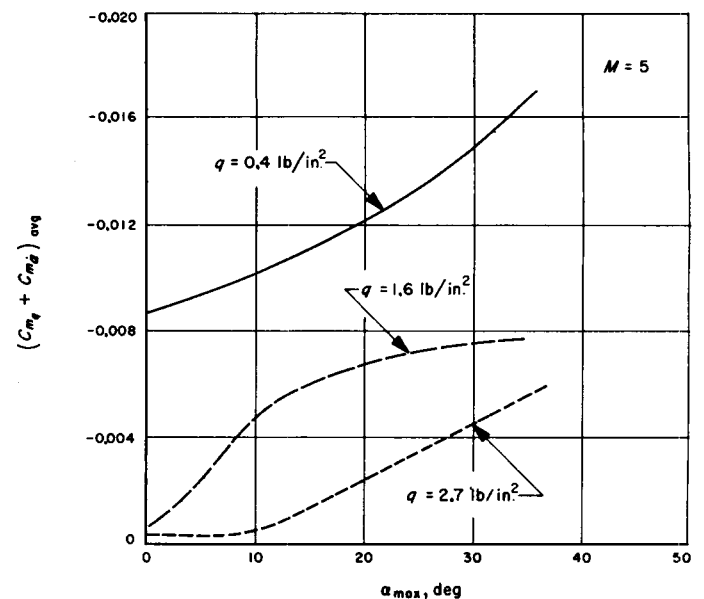


Fig. 29. Sting-support gas bearing as measured with a calibration sphere, at various dynamic pressures

oscillation, while the cross-supported system exhibits a fairly constant level of damping with angle of oscillation. Before this difference in damping of the sphere can be attributed to the presence of the base slot, additional investigation should be carried out. However, in terms of the model aerodynamic-pitch-damping coefficient, this difference is small and repeatable, so there should be no problem in correcting the damping data for the bearing damping.

For a first approximation, the magnitude (not the dimensionless coefficient) of the gas-bearing damping is independent of the load applied—until the bearing is grounded out. As a consequence, using the nondimensionalizing procedure, the values of bearing damping $(C_{m_q} + C_{m_{\dot{\alpha}}})_{\text{avg}}$ are inversely proportional to the tunnel dynamic pressure. An example of the sting-supported air-bearing damping coefficient as a function of tunnel dynamic pressure is shown in Fig. 29.

VII. CONCLUSIONS

If the aerodynamic pitch damping of certain short, blunt vehicles entering the Mars atmosphere is unfavorable, even if very small, the oscillatory motion will become divergent after the region of maximum deceleration. Prior to this region the effects of pitch damping are negligible. The effect of vehicle shape upon the oscillatory motion is very strong, and is directly related to the ratio C_{L_α}/C_D when constraints are imposed to make the vehicle diameter, ballistic coefficient, moment of inertia, and pitching-moment slope at zero angle of attack independent of shape.

It is shown that there is a considerable spread in the pitch-damping coefficient ($C_{m_q} + C_{m_\alpha}$) effect on the angle-of-attack envelopes for the shapes considered; the higher the ratio C_{L_α}/C_D , the less the effect of pitch damping. Also, the shapes with the higher C_{L_α}/C_D ratio are less dependent upon pitch damping in order to maintain angle-of-attack stability. The minimum point on the oscillatory envelope for critically damped motion appears to be the same for all shapes—about 20 to 25 deg.

By the time the vehicle's velocity is low enough to permit parachute deployment, the amplitude of the oscillation could be large enough to prevent reliable deployment. Therefore it becomes necessary to accurately measure the magnitude and sign of the aerodynamic pitch damping of each likely entry-vehicle shape at large amplitudes of oscillation. These entry trajectory studies give an insight as to the pitch-damping accuracies and angle-of-attack amplitudes required for the experimental measurements. The usual means (such as ballistic range firing, sting-flexure models, sting- and cross-support ball-bearing suspended models) are not adequate for the measurement of the expected low pitch damping at high

angles of oscillation for the short, blunt vehicle shapes being considered for entry into the atmosphere of Mars.

Both sting-support and cross-support gas-bearing mounted models can adequately measure the small pitch damping because of their relatively low friction and the inherent repeatability of the data. The use of free-flight testing in a wind tunnel has been proposed as a companion method to the gas-bearing approach in order to assess sting- and cross-support interference on the model pitch damping. Not only is it practical to calculate average effective pitch damping (which remains constant for all angles during each half cycle of oscillation and is only a function of the amplitude of oscillation of that particular half cycle of motion), but the use of this average value yields adequate oscillation amplitude-decay rates for the single-degree-of-freedom equation-of-motion studies. There does not appear to be any reason why this same conclusion should not be the case for both single-plane and six-degree-of-freedom rigid-body motions.

Finally, in addition to the possibility of being able to obtain support-interference-free pitch-damping data, the wind-tunnel free-flight technique can be used to study, in detail, model oscillatory motion through a very large range of model mass characteristics and tunnel operating conditions. This should serve to validate or indicate the limitations in the application of experimental data and the consequent use of these data in the six-degree-of-freedom equations-of-motion studies. The ability to design a model and pick the proper tunnel operating conditions makes it practical to experimentally duplicate or simulate several important characteristics of the motion expected during the latter portion of an atmosphere-entry trajectory.

NOMENCLATURE

A	model reference area = $\pi d^2/4$	R_D	freestream Reynolds number based on model reference diam
C_D	drag coefficient = D/qA	t	time
C_L	lift coefficient = L/qA	V	freestream velocity for model test or vehicle flight velocity
$C_{L\alpha}$	lift coefficient slope per rad	V_E	vehicle velocity with respect to atmosphere at 800,000 ft altitude
C_m	pitching-moment coefficient = M/qAd	y	altitude
$C_{m\alpha}$	pitching-moment coefficient slope per rad	α	angle of attack of model axis of symmetry relative to tunnel freestream velocity or flight vehicle axis of symmetry relative to nominal trajectory
$(C_{m_q} + C_{m\dot{\alpha}})$	pitch-damping coefficient = $M_D/(qAd^2/V)$	α_{env}	envelope of oscillatory motion
$(C_{m_q} + C_{m\dot{\alpha}})_{avg}$	average effective pitch-damping coefficient as determined from f and $\Delta\alpha/\alpha_{max}$ by use of Eq. (15)	α_{max}	any α where $\dot{\alpha} = 0$ (see Section IV. A. for schematic)
$(C_{m_q} + C_{m\dot{\alpha}})_{crit}$	critical pitch-damping coefficient (see text)	α_0	the α_{max} where $t = 0$
d	model reference diam (maximum cross-section diam)	α'	angle of attack as measured from pictures such as in Fig. 20
D	drag	$\Delta\alpha$	the decay in α_{max} during one cycle of oscillation
f	oscillation frequency in cps	β	reciprocal of the atmosphere scale height
I	moment of inertia of body about axis of oscillation (center of gravity)	ρ_0	reference atmospheric density
L	lift	θ_E	vehicle path angle at 800,000 ft altitude with respect to the local horizon
m	mass of model	ω	angular velocity in rad/sec
M	Mach number	ψ_B'	angle of yaw inferred from model "base bulge" measurement from pictures such as in Fig. 20
M	static-pitching moment		
M_D	pitch-damping moment per rad/sec		
M_α	slope of the pitching moment per rad		
q	freestream dynamic pressure		

REFERENCES

1. Peterson, V. L., *Motions of a Short 10° Blunted Cone Entering a Martian Atmosphere at Arbitrary Angles of Attack and Arbitrary Pitch Rates*, National Aeronautics and Space Administration, NASA TN D-1326, May, 1962.
2. Allen, H. J., *Motion of a Ballistic Missile Angularly Misaligned with the Flight Path Upon Entering the Atmosphere and its Effect upon Aerodynamic Heating, Aerodynamic Loads, and Miss Distance*, National Advisory Committee for Aeronautics, NACA TN 4048, October, 1957.
3. Brofman, W., *Aerodynamic Stability of Planetary Entry Vehicles*, Technical Report No. 32-338, Jet Propulsion Laboratory, Pasadena, California, September, 1962.
4. Fletcher, H. S., and W. D. Wolhart, *Damping in Pitch and Static Stability of Supersonic Impact Nose Cones, and Manned Reentry Capsules at Mach Numbers from 1.93 to 3.05*, National Aeronautics and Space Administration, NASA TM X-347, November, 1960.
5. Wehrend, W. R., Jr., *Wind Tunnel Investigation of the Static and Dynamic Stability Characteristics of a 10° Semivertex Angle Blunted Cone*, National Aeronautics and Space Administration, NASA TN D-1202, 1962.
6. Intrieri, P. F., *Free-Flight Measurements of the Static and Dynamic Stability and Drag of a 10° Blunted Cone at $M = 3.5$ and 8.5* , National Aeronautics and Space Administration, NASA TN D-1299, 1962.
7. Shantz, I., and R. T. Groves, *Dynamic and Static Stability Measurements of the Basic Finner at Supersonic Speeds*, NAVORD Report 4516, Naval Ordnance Laboratory, White Oak, Maryland, January, 1960.
8. Welsh, C. J., L. K. Ward, and R. H. Urban, *Damping Measurements with a Sting-Supported Bearing-Pivot Dynamic Balance*, AEDC-TN-61-52, Arnold Engineering Development Center, Tullahoma, Tenn., May, 1961.
9. Allen, H. J., and A. J. Eggers, Jr., *A Study of the Motion and Aerodynamic Heating of Missiles Entering the Earth's Atmosphere at High Supersonic Speeds*, NACA TN 4047, National Advisory Committee for Aeronautics, October, 1957.
10. Babineaux, T. L., D. A. Nelson, and B. Dayman, *A Technique for Obtaining Dynamic Stability Derivatives at Large Angular Amplitudes*, WT G-T15, Jet Propulsion Laboratory, Pasadena, California, April, 1962.
11. Shantz, I., R. T. Groves, F. DeMeritte, *Pitch-Damping Wind-Tunnel Tests of the Jupiter Re-Entry Body*, NAVORD Report 6053, Naval Ordnance Laboratory, White Oak, Maryland, February, 1958.
12. Dayman, B., *Optical Studies of Free-Flight Wakes*, Technical Report No. 32-364, Jet Propulsion Laboratory, Pasadena, California, November, 1962.
13. Nelson, R. L., *Measurement of Aerodynamic Characteristics of Re-Entry Configurations in Free Flight at Hypersonic and Near-Orbital Speeds*, North Atlantic Treaty Organization, Advisory Group for Aeronautical Research and Development, Report 380, July, 1961.
14. Dayman, B., *Simplified Free-Flight Testing in a Conventional Wind Tunnel*, Technical Report No. 32-346, Jet Propulsion Laboratory, Pasadena, California, October, 1962.
15. Staff, *Wind Tunnel Facilities at the Jet Propulsion Laboratory*, Technical Release No. 34-257, Jet Propulsion Laboratory, Pasadena, California, January, 1962.
16. Nelson, D. A., *Results of the JPL Aerodynamic Damping-in-Pitch Wind Tunnel Program*, WT 20-499, Jet Propulsion Laboratory, Pasadena, California, November, 1962.
17. Nelson, D. A., *Aerodynamic Stability Test of the North American Aviation, Inc. Apollo Models*, WT 20-516, Jet Propulsion Laboratory, Pasadena, California, November, 1962.